BRNO UNIVERSITY OF TECHNOLOGY

VYSOKÉ UČENÍ TECHNICKÉ V BRNĚ

FACULTY OF CHEMISTRY

FAKULTA CHEMICKÁ

INSTITUTE OF MATERIALS SCIENCE

ÚSTAV CHEMIE MATERIÁLŮ

INFRARED SPECTROSCOPY OF THIN FILMS

INFRAČERVENÁ SPEKTROSKOPIE TENKÝCH VRSTEV

BACHELOR'S THESIS

BAKALÁŘSKÁ PRÁCE

AUTHOR — Andrej Kiss

AUTOR PRÁCE

SUPERVISOR — prof. RNDr. Vladimír Čech, Ph.D.

VEDOUCÍ PRÁCE

BRNO 2020

BRNO UNIVERSITY OF TECHNOLOGY
FACULTY OF CHEMISTRY

Specification Bachelor's Thesis

Project no.:	FCH-BAK1471/2019	Academic year:2019/20
Department:	Institute of Materials Science	
Student:	**Andrej Kiss**	
Study programme:	Chemistry and Technology of Materials	
Study branch:	no specialisation	
Head of thesis:	**prof. RNDr. Vladimír Čech, Ph.D.**	

Title of Bachelor's Thesis:

Infrared spectroscopy of thin films

Bachelor's Thesis:

–Background research in plasma–enhanced chemical vapor deposition (PECVD) and infrared spectroscopy.
–Practical skills in measurements of transmission infrared spectra for thin film on silicon wafer; design of spectra interpretation.
–Determination of chemical structure of silicon–based thin films depending on deposition conditions.

Deadline for Bachelor's Thesis delivery: 31.7.2020:

Bachelor's Thesis should be submitted to the institute's secretariat in a number of copies as set by the dean This specification is part of Bachelor's Thesis

Andrej Kiss	prof. RNDr. Vladimír Čech, Ph.D.	doc. Ing. František Šoukal, Ph.D.
student	Head of thesis	Head of department

prof. Ing. Martin Weiter, Ph.D.
Dean

In Brno dated 31.1.2020

ABSTRACT

The objective of this Bachelor thesis is a literary research in the fields of thin films, plasma enhanced chemical vapor deposition technique, and Fourier transform infrared spectroscopy in order to measure the infrared spectra of thin films and characterise its chemical structure based on the measured spectra. Five samples of plasma polymer films of tetravinylsilane, deposited on silicon wafers using plasma enhanced chemical vapor deposition with effective power ranging from 2 to 150 W were measured with Fourier transform infrared spectroscope. The measurement revealed the chemical bonds present in the five samples and how the structure changed with changing effective power. The decrease in the absorption bands with hydrogen presence suggest an increase of crosslinking with enhanced power. Also, the decrease in the band with silicon presence provides evidence for the increase of C/Si ratio. These results help us understand the characteristics of these thin films and contribute to the understanding the plasma enhanced chemical vapor deposition process.

ABSTRAKT

Cílem této bakalářské práce je literární rešerše v oblasti tenkých vrstev, plazmochemické depozice z plynné fáze a infračervené spektroskopie Fourierovou transformací, a měření infračervených spekter tenkých vrstev a charakterizace jejich chemické struktury na základě změřených spekter. Pomocí infračervené spektroskopie Fourierovou transformací bylo měřeno pět vzorků tenkých polymerních vrstev z tetravinylsilanu, vytvořených na křemíkovém substrátu pomocí plazmochemické depozice z plynné fázi s efektivním výkonem v rozmezí od 2 W do 150 W. Měření odhalilo chemické vazby přítomné ve vzorcích a jak se struktura měnila s měnící se efektivním výkonem. Snížení absorpčních pásů s přítomností vodíku naznačuje zvýšení zesítění se zvýšeným efektivním výkonem. Také snížení absorpčních pásů s přítomností křemíku poskytuje důkaz pro zvýšení poměru C/Si. Tyto výsledky nám pomáhají porozumět charakteristikám těchto tenkých vrstev a přispívají k pochopení procesu plazmochemické depozice z plynné fáze.

KEYWORDS

Thin films, plasma polymerisation, PECVD, tetravinylsilane, Fourier transform infrared spectroscopy (FTIR).

KLÍČOVÁ SLOVA

Tenké vrstvy plazmová polymerace, PECVD, tetravinylsilan, infračervená spektroskopie s Fourierovou transformací (FTIR).

KISS, Andrej. *Infračervená spektroskopie tenkých vrstev.* Brno, 2020. Dostupné také z: https://www.vutbr.cz/studenti/zav-prace/detail/122334. Bakalářská práce. Vysoké učení technické v Brně, Fakulta chemická, Ústav chemie materiálů. Vedoucí práce Vladimír Čech.

DECLARATION

I declare that the diploma thesis has been worked out by myself, under leadership of my supervisor and then all the quotations from the used literary sources are accurate and complete. The content of the diploma thesis is the property of the Faculty of Chemistry of Brno University of Technology and all commercial uses are allowed only if approved by both the supervisor and the dean of the Faculty of Chemistry, BUT.

.....

author's signature

ACKNOWLEDGEMENT

I would like to thank my bachelor's thesis supervisor prof. RNDr. Vladimír Čech, Ph.D. for professional guidance, consultations, and valuable advice at processing of this work. Furthermore, my thanks go to Naghmeh Aboualigaledari for all her help, expert interpretation, getting acquainted with the deposition apparatus and infrared spectroscopy in practice.

CONTENTS

1 INTRODUCTION

This work focuses on the characterization of thin films by Fourier transform infrared spectroscopy. Plasma polymer thin films of tetravinylsilane were prepared with the plasma enhanced chemical vapour deposition method.

Plasma enhanced chemical vapour deposition method allows us to prepare thin films with the desired physicochemical properties depending on deposition conditions. This nature of the method results in a range of useful applications of these thin films such as barrier coatings, corrosion protection, chemical sensors, or functional interlayers in polymers. Because of the wide range of applications, these thin films are subject to multiple researches focusing on chemical and physical properties.

The first part of this work focuses on the theoretical introduction of the thin films, the PECVD preparation method and description of the FTIR spectroscopy as a tool for the characterization of the thin films. The experimental part describes the deposition system and FTIR spectroscopy, introduce the used materials and details the deposition steps and infrared measurement. The final part of this work outlines how data was processed and describes the chemical structural changes in the prepared film samples.

2 THEORETICAL PART

2.1 Thin films

Thin film is one of the most versatile technologies, with thin solid films having a wide variety of functions and applications. Thin films were first studied in the context of optical phenomena but today we are most interested in their other unique properties and uses, especially in the development of miniature and highly integrated semiconductors, and in their use in surface coatings to protect materials [1–3].

It is important to define what a film is from the perspective of its geometrical structure: a film is a layered structure, with one of its dimensions being considerably smaller than the other two. Figure 1 shows the dimension differences [2].

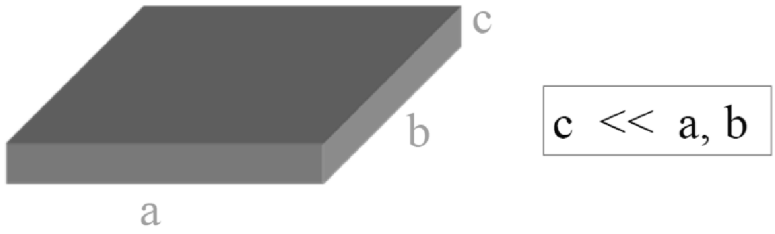

Figure 1: Model of layer type structure

In addition, if we talk about a thin film it is also important to specify what do we consider to be thin. A thin layer means that the two surfaces of the material are so close that the physical properties of it are changed. This is caused by most of the atoms in the material being on the surface and their cohesion affects the structure of the material This structural alteration changes the mechanical properties, the electrical conductivity, the melting point, and the optical properties The usual thickness of these layers is between 0,1 nm and 10 μm. A thin film can be made from organic, inorganic, or hybrid materials having a crystalline, polycrystalline, or amorphous structure [2,3].

One of the fastest ways to identify whether a material has a thin layer on the surface is by examining light interference on the surface. Light interference manifests in the formation of interference colours on the surface. This effect is created by the reflected light from the surface of the thin layer and from the surface of the main material. Between these two lights, the beams differ in path and phase which creates interference. If these light beams meet in the same phase, the interference is constructive, if they meet in the opposite phase, then the interference is destructive [4].

For some applications, we must classify thin films based on the type of their geometrical configuration. This helps to better understand the properties of these systems. The configurations are termed film, line, or island. These configurations can also be subdivided based on their confinement into unconfined, partially confined, and fully confined, as shown in Figure 2. In a one atomic layer a film is sometimes referred to as two-dimensional matter, a line is a one-dimensional matter and a dot a zero-dimensional matter [1].

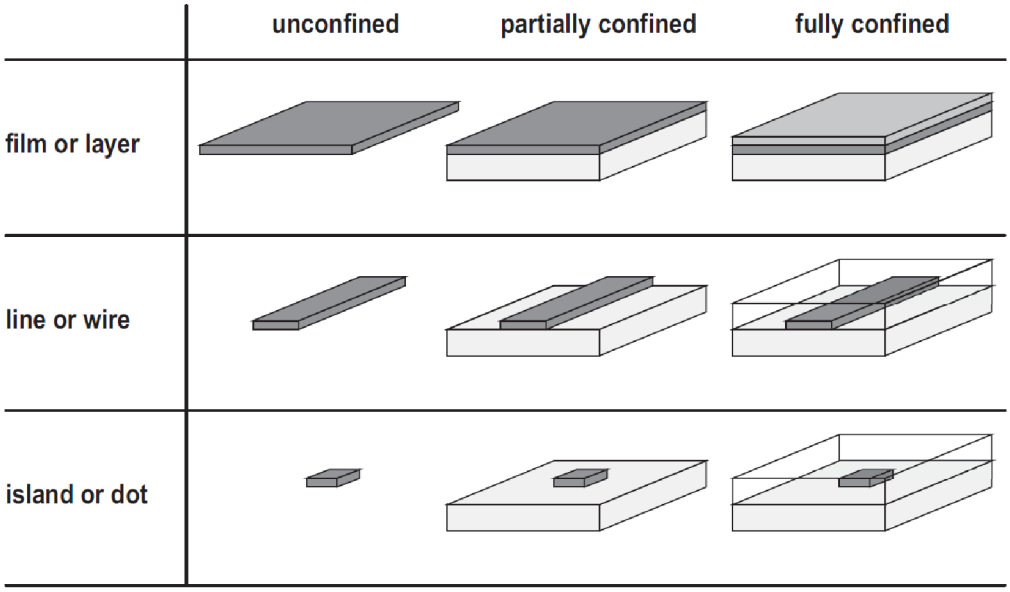

Figure 2: Classification of thin-film configuration[1].

2.1.1 The technology of thin-film preparation

The preparation methods of thin-films can be divided into two major groups with different principles. The first one is physical vapor deposition (PVD) which is based on a physical process, and the second one is chemical vapor deposition (CVD) which in contrast is based on a chemical reaction. Some methods, however, can not be classified into any of these groups, because they are using a specific method which uses both principles. This is sometimes referred to as the reactive PVD process [1,5].

PVD can be implemented in numerous ways. Each method usually differs in how the material is deposited, how it enters the vapor phase, and what engineering implementations are used. The most used physical methods for preparing thin films include pulsed laser deposition (PLD), vacuum evaporation, and sputtering. PLD is based on a high-power pulsed laser beam which is focused inside a vacuum to strike the target material. This material is vaporized then deposited as a thin film on a substrate. The next method is vacuum evaporation: in this method the desired material is evaporated by heating to a high temperature in a vacuum. The vapour of the material then condenses and solidifies on the surface. The sputtering method requires high energy ions or particles, generated by electrical discharge in an inert gas at low pressure and high voltage. There are many different sputtering methods, used in different applications: DC such as: sputtering, radio frequency sputtering, magnetron sputtering [1,6].

The chemical vapor deposition uses a chemical reaction of volatile compounds to form a non-volatile thin film. Figure 3 shows the basic steps. This process differs from the PVD processes, as it does not require vacuum or power electrical sources. The high-temperature CVD processes are widely used for creating coatings in many technologies such as in the field of electronics, and in the production of ball bearings, machine tools, rocket motors and reactor components [2].

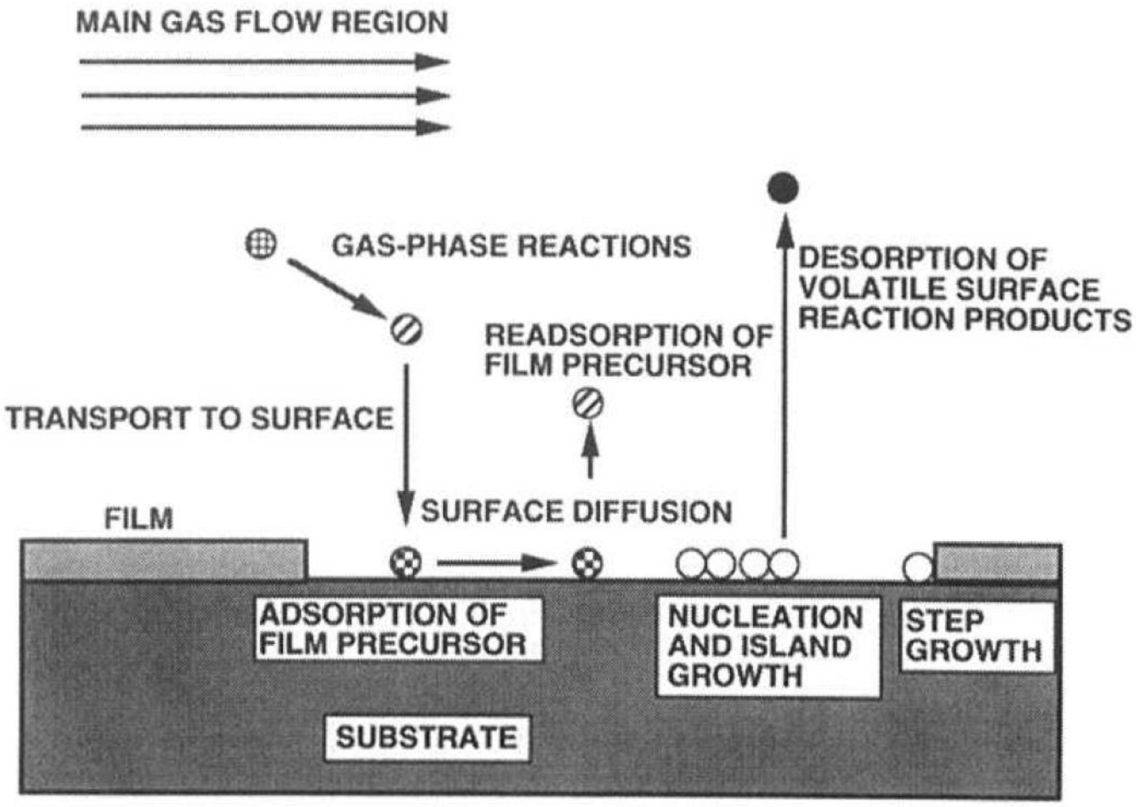

Figure 3: Reaction process of CVD film growth [2].

This method can produce different films of organic and inorganic compounds, metals, and semiconductors with desirable properties. Various modified equipments can be used to overcome some of the technical difficulties of the conventional CVD process, including the following: hot filament CVD (HFCVD), plasma-enhanced CVD (PECVD), atmospheric pressure CVD (APCVD), low-pressure (LPCVD), laser-enhanced CVD (LECVD) [2].

2.1.2 Plasma enhanced chemical vapor deposition

Plasma-enhanced chemical vapor deposition is used to create thin films. In this process a film deposition is occurs by glow discharge initiated chemical reaction. Because of the characteristics of this method it possible to control the composition and microstructure [2].

2.1.2.1 Plasma

Plasma is an ionized gas and the fourth state of matter after solid, liquids, and gas states. Figure 4 displays the transition process. Ionized here means that one or more electrons are detached from the atoms that make up the material, and thus the plasma becomes a mixture of ions and free electrons. Because the electrons are no longer attached to atoms but can move freely in the plasma, the plasma becomes electrically conductive and interacts with electromagnetic fields. Plasma is much more common in the universe than usually thought, in fact, 99 % of the matter in the visible universe is in this state. The plasma state only begins to form at very high temperatures, around ten thousand kelvins, because only in those conditions is there enough energy to tear off electrons [7].

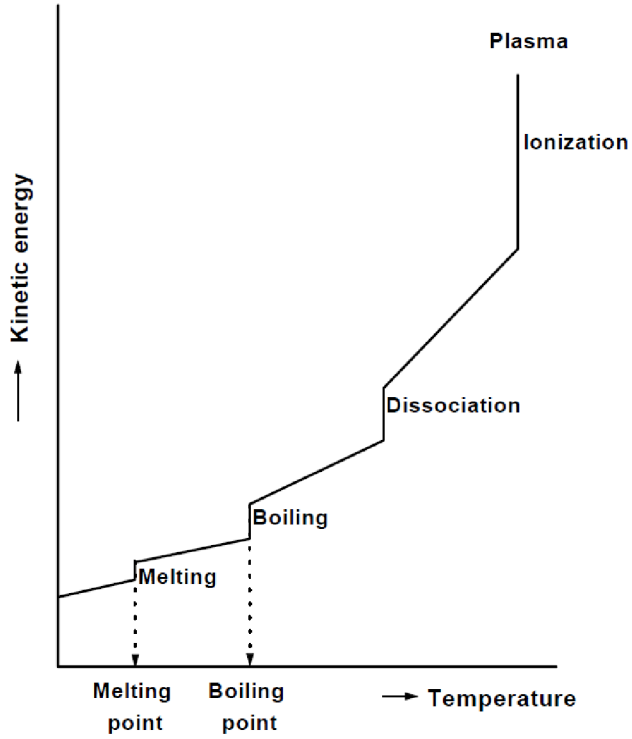

Figure 4: Schematic diagram of the state transition process [7].

Plasma can be obtained by raising the temperature of a matter until a reasonably high ionization is produced. In the thermodynamic equilibrium, the degree of ionization and the electron temperature are related. By the degree of ionization, we can divide plasma into weakly ionized and strongly ionized plasma. In weakly ionized plasma the density of charged particles is negligible compared to the density of neutral molecules (atoms). Thus, the charged particles predominantly collide with the neutral molecules. In strongly ionized plasma the density of charged particles predominates. Thus, charged particle collisions dominate. This plasma classification characterizes the physical properties of the plasma. The nature of the electrical conductivity of a plasma greatly depends on whether the plasma is weakly or strongly ionized. In the case of weakly ionized plasma, the electrical conductivity of plasma increases with the concentration of the charged particles. At a constant concentration of charged particles, the electrical conductivity decreases with increasing electron temperature. In the case of strongly ionized plasma, the electrical conductivity does not depend on the concentration of the charged particles and increases with the temperature of the electrons [8,9].

2.1.2.2 Mechanism of plasma polymerization.

To understand the mechanism of PECVD it is important to know the underlying process of plasma polymerization. Plasma polymerization is a process in which a polymer is formed from a monomer placed in plasma discharge under certain deposition conditions. It is, however, not a classical type of polymerization: plasma polymerization differs from conventional polymerization such as radical or ionic polymerization. The term radical or ionic polymerization refers to the type of particles that are responsible for propagation reactions. The term plasma polymerization refers to the source by which the polymerization reactions are

initiated. The plasma polymers are created by an atomic process. The monomer is fragmented, and mainly new covalent bonds are formed between the atoms. Materials prepared by plasma polymerization differ significantly from conventional polymers and differ from most inorganic materials. Their great advantage is their insolubility and infusibility. Plasma polymers are usually highly branched and highly crosslinked [7].

The preparation of a conventional polymer consists of many steps. In the case of a plasma polymer, all the functional steps are replaced by a one-step process. The process of forming a thin layer of plasma polymer consists of three different steps which are shown in Figure 5:

1. Plasma activation of a molecule by electron impact dissociation.
2. Transport of generated radicals to the substrate.
3. The chemical reaction of formed radicals on the surface of the plasma polymer layer [7,10].

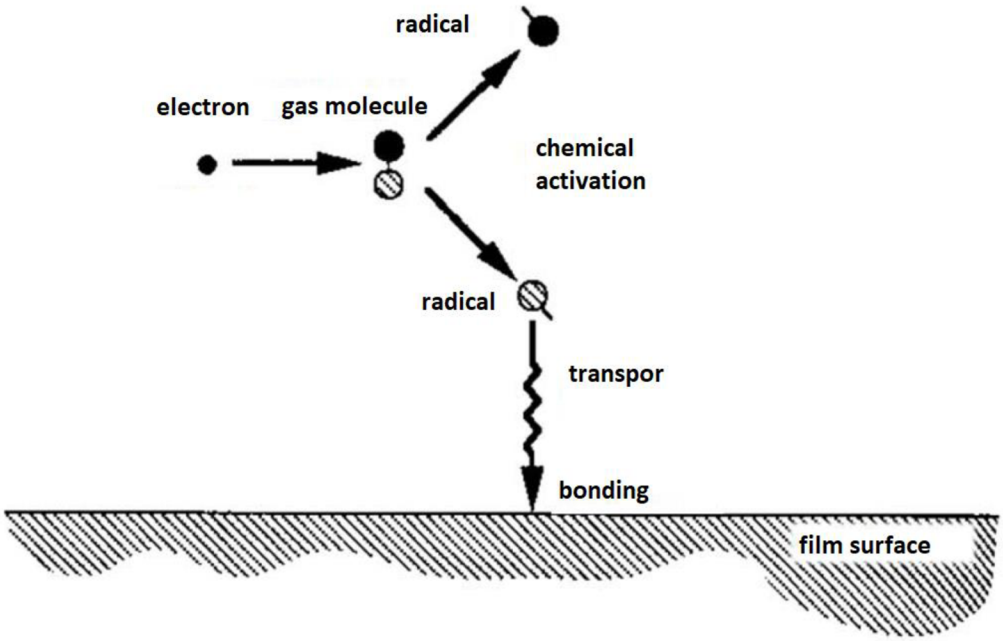

Figure 5: Thin-film forming process by plasma polymerization [10].

The plasma polymerization reaction mechanism is shown in Figure 6 which was proposed by Yasuda. Mi represents a neutral particle, which may be a molecule of the original monomer or one of the dissociation products. Then this neutral particle is activated by the elimination of a hydrogen atom with electrons, to form a monoradical M• or a biradical •M•. The indices i, j, and k indicate different particle sizes. Then the reaction can proceed six different ways: A monoradical Mi• can connect to a neutral monomer to form Mi-M• this is reaction 1. Mi• can connect to another monoradical Mj• to form a neutral molecule Mi-Mj this is reaction 2, it can also connect with a biradical •Mk• to form a new monoradical Mi-Mj• this is reaction 3 and 5. The biradical •Mk• can react with a neutral monomer to form a new biradical •Mk-M• this is reaction 4. •Mk• can also recombine with a biradical •Mj• and form a new biradical •Mk-Mj• this is reaction 6. The newly formed neutral molecule Mi-Mj is reactivated by plasma and forms a monoradical or biradical, see cycle 1. The new monoradicals Mi-Mk• and biradicals •Mk-Mj• further recombine and form larger radicals, see cycle 2 [7,10].

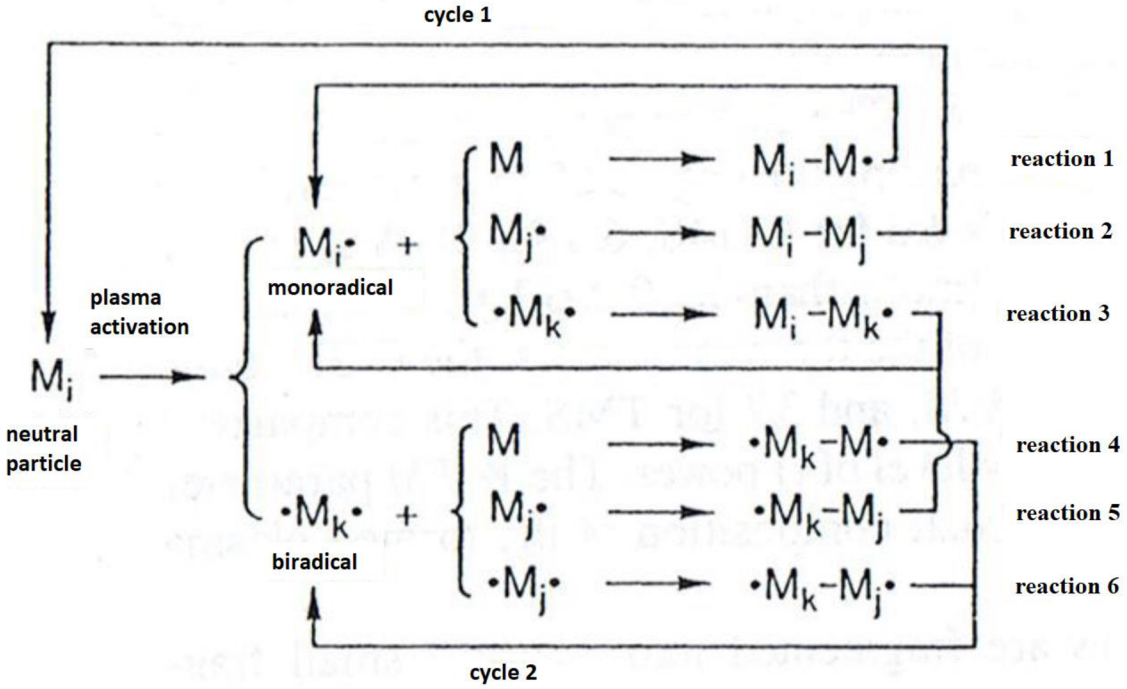

Figure 6: Reaction mechanism of plasma polymerization [10].

2.1.2.3 Organosilicon thin films

Organosilicon thin films have a wide variety of properties because of different monomers and deposition parameters. Also, organosilicons are relatively nontoxic, nonflammable, and cheap. An organosilicon monomer is a complex molecule composed of at least one Si atom and other organic groups. The main organosilicon monomers for thin-film preparation are shown in Table 1 [11].

Table 1: Selected organosilicates used in plasma polymerization

Name	Formula	Reference
Hexamethyldisilane	$(CH_3)_3Si\text{-}O\text{-}Si(CH_3)_3$	[12]
Tetraethoxysilane	$(C_2H_5\text{-}O)_4Si$	[13]
Tetramethyldisiloxane	$H\text{-}Si(CH_3)_2\text{-}O\text{-}(CH_3)_2Si\text{-}H$	[14]
Tetramethylsilane	$Si(CH_3)_4$	[15]
Tetravinylsilane	$(CH_2{=}CH)_4Si$	[16]
Hexamethyldisilane	$(CH_3)_3Si\text{-}Si(CH_3)_3$	[17]
Oktamethylcyklotetrasiloxan	$Si_4O_4(CH_3)_8$	[18]

2.1.3 Application of thin films.

Properties and the preparation of thin layers varies widely, as a result, thin films have comprehensive utilization. The main applications of thin films are [19]:

- optically functional: laser optics, reflective and antireflective coating, optically absorbing materials, transparent conductive films
- energy related: thin film battery, thin film fuel cell electrochromic coating, solar absorbers, organic solar cells, photocatalytic coatings
- electrically functional: electrical conductors, semiconductor films, insulators, photovoltaics
- chemically functional: corrosion-resistant coatings, catalytic coatings biomedical coatings, thin film electrolytes, organic materials
- mechanically functional: lubrication films nanocomposites, diffusion barriers, hard coatings for cutting tools, wear-resistant coatings, biomedical coatings

2.2 Infrared spectroscopy

The subject of spectroscopy is the study of the interaction (emission, absorption, scattering) between matter and electromagnetic wave. If we are studying the electromagnetic wave emitted by the object, we are talking about emission spectroscopy. Absorption spectroscopy is when the object absorbs electromagnetic radiation and increases its internal energy [20].

In infrared spectroscopy, the sample is irradiated with electromagnetic radiation in the infrared wavelength (780 nm – 1 000 μm, which corresponds to wavenumbers 12 000 – 10 cm^{-1}) we can measure the change in the absorbed, emitted, or reflected radiation modified by the molecular properties of the sample [21].

The wavenumber is related to the wavelength by

$$\tilde{\nu} = \frac{1}{\lambda}, \tag{1}$$

where $\tilde{\nu}$ is the wavenumber (m^{-1}), λ is the wavelength (m), and to the frequency by:

$$\tilde{\nu} = \frac{\nu}{c}, \tag{2}$$

where ν is the frequency (Hz) and c is the speed of light in a vacuum ($m \cdot s^{-1}$) [22].

The electromagnetic spectrum is shown in Figure 7. Infrared radiation can be further divided into three regions. Near infrared (NIR), which connects to the visible light: 780 – 2 500 nm or 12 000 – 4 000cm^{-1}. Middle infrared (MIR) 2,5 – 50 μm or 4 000 – 200 cm^{-1}. Far infrared (FIR): 50– 1 000 μm or 200 – 10 cm^{-1}. For analytical purposes, the most used region is the MIR, which can be further divided into the fingerprint region 1 500 – 300 cm^{-1} and the functional group region 4 000 – 1 500 cm^{-1} [20,23].

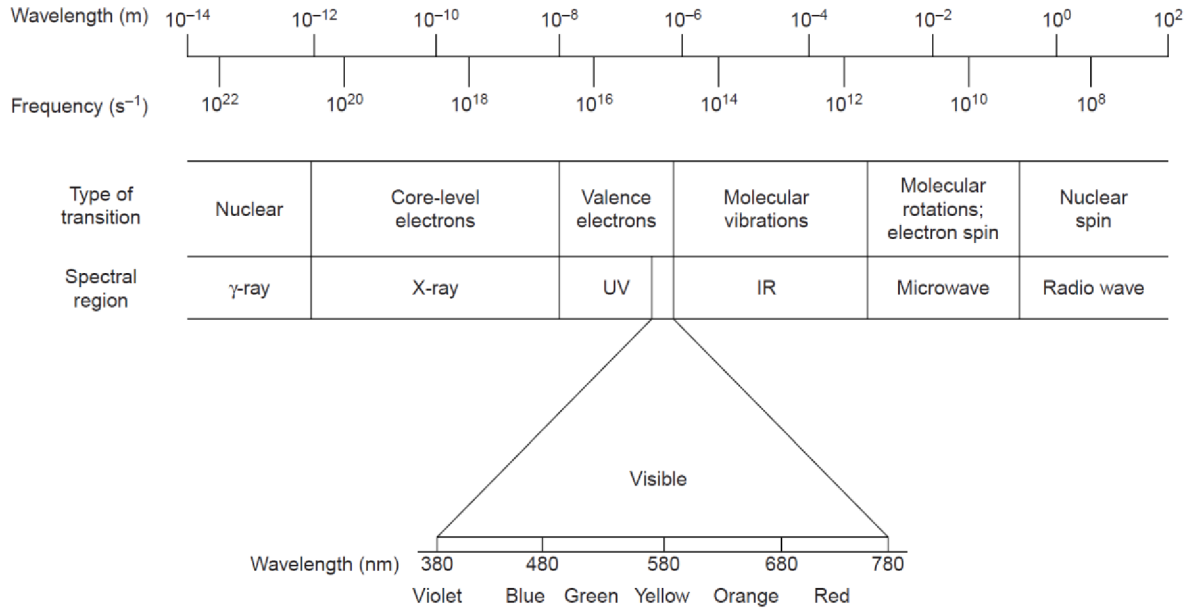

Figure 7: The electromagnetic spectrum [24]

2.2.1 Principles of infrared spectroscopy

The basic principle is that the energy of infrared radiation is not sufficient to excite an electron in molecular orbitals, but it is sufficient to change the vibration or the rotational state of a molecule. From the point of view of classical physics, the vibrational motion can be understood as a periodic change of the internuclear distance between individual atoms. In general, an *n* atomic molecule has *3n* degrees of freedom. Three of them are intended for the translational motion of the center of gravity of the molecule in the direction of the *x*, *y,* and *z* axes, and the other three are intended for the description of its rotational motion. In the case of a linear molecule, these are only two directions, where the two rotational moments in the direction of the *x*, *y,* and *z* axes are identical. The number *3n–6* (*3n–5* in the case of a linear molecule) therefore remains for the vibrational movements of the molecule. In the case of a diatomic molecule, there is a single vibrational degree of freedom due to the stretching of the bond between the two atoms [21,22,25].

A simple description of the movement is expressed using a formula:

$$q = r\text{-}r_e, \tag{3}$$

where *r* is the instantaneous and r_e is the equilibrium bond length, *q* represents the vibrational coordinate, which can be used to describe the valence vibration in this diatomic molecule. Using these vibrational coordinates, the energy associated with the vibrational motion can be expressed. As the molecule performs a vibrational motion, energy is transferred between the kinetic and potential forms. The potential energy, therefore, changes depending on the size of the vibration coordinate *q* and the graphical expression of this dependence is the so-called potential energy curve Figure 8 [21,22,25].

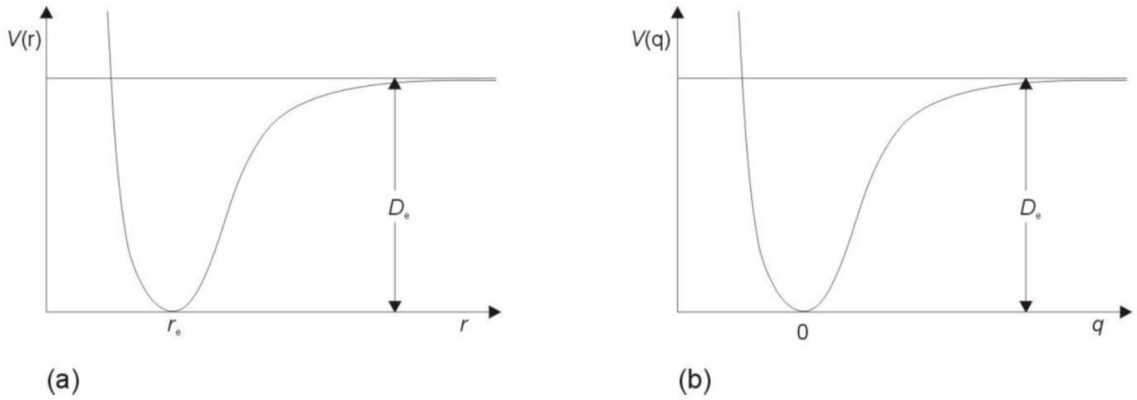

Figure 8: Vibration potential energy V as a function of (a) bond length (b) vibration coordinates [22].

The shape of the potential curve shows that at small internuclear distances the molecular energy increases rapidly due to strong repulsion between the charged particles, conversely at extremely large distances the bond ruptures. In this limiting case, the potential energy acquires a constant value corresponding to the sum of the energies of the two independent atoms the process is called dissociation of the bond and it denoted by the dissociation energy D_e. If the potential energy curve of a vibrating molecule can be approximated by a parabola, we speak of vibrational motion as a harmonic oscillator [22].

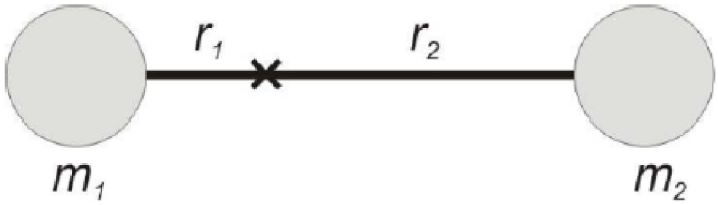

Figure 9: A diatomic molecule as a harmonic oscillator
where the center of gravity is represented by *x* [22].

According to classical mechanics, a harmonic oscillator is two mass points connected by a spring, shown in Figure 9, the force which returns atoms to equilibrium can be written as:

$$\mathrm{F} = -\mathrm{k} \cdot x, \tag{4}$$

where *F* is the force, *k* is the potential constant and *x* is the deviation of the atoms from the equilibrium position. The potential energy *V* of this system can be obtained by integrating equation (4):

$$\mathrm{V} = \frac{1}{2}\mathrm{k} \cdot \mathrm{x}^2. \tag{5}$$

According to this equation, the potential energy curve has the shape of a parabola [22].

Classical mechanics provides a basic idea of the frequency of vibrating atoms in a molecule, according to which the energy of an oscillator can take on any value. However, the energy of a vibrating molecule cannot take on any arbitrary value, but it is quantized this is shown in Figure 10, which results from the solution of the Schrödinger equation:

$$-\left(\frac{\hbar^2}{2\mu}\right) \cdot \frac{\partial^2 \psi_v}{\partial q^2} + \frac{1}{2} k q^2 \psi_v = E_v \psi_v. \tag{6}$$

By solving this second-order differential equation, we get the energy of individual vibrational states E_{vib}:

$$E_{vib} = \left(v + \frac{1}{2}\right) hv, \tag{7}$$

where v is a vibrational quantum number that can only take on the values 0, 1, 2, 3…., *h* is Planck's constant and v is the frequency of the vibrating molecule expressed in hertz. The frequency we can get form the solution of Hooke's law:

$$v = \frac{1}{2\pi} \cdot \sqrt{\frac{k}{\mu}}, \tag{8}$$

where *k* is the potential constant and μ is the reduced mass of vibrating atoms:

$$\mu = \frac{m_1 \cdot m_2}{(m_1 + m_2)}, \tag{9}$$

m_1 and m_2 are the masses of the vibrating atoms [22,25].

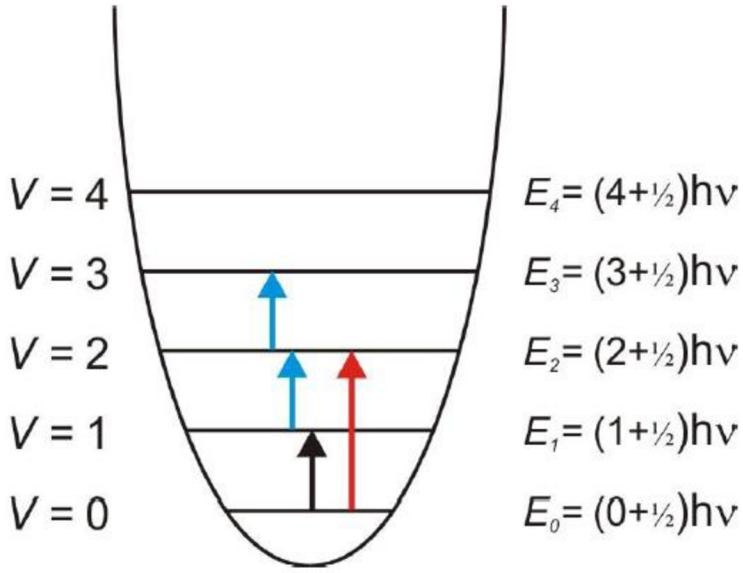

Figure 10: Representation of energy levels and vibrational transitions of a harmonic oscillator [22].

In infrared spectroscopy, a molecule can only absorb radiation when the incoming infrared radiation is of the same frequency as one of the fundamental modes of vibration of the molecule. This results in an infrared spectrum from which it is possible to determine the structure of the molecule. From the point of view of classical physics point of view, the vibration motion can be symmetric and antisymmetric stretching, scissoring, wagging, and twisting [21].

Certain factors may complicate the infrared spectra. The first one is *overtone bands* that arise from the absorption of a photon leading to a direct transition from the ground state to the second excited vibrational state. Since the energy is of the absorbed frequency is proportional to the wavenumber, the first overtone will appear in the spectrum at twice the wavenumber of the fundamental. *Combination bands* emerge when two fundamental bands absorbing energy simultaneously. The resulting band will appear at the sum of the two bands wavenumber. If only one band is expected and, but it is appearing in two bands close together this is the *Fermi resonance*. It is a consequence of quantum mechanical wavefunction mixing.

The *coupling* is when the vibrating bonds are joined to a single, central atom this is resulting in the same number of vibrational modes, but at different frequencies, and bands can no longer be assigned to one bond. These factors can result in the misinterpretation of the bands [21].

2.2.2 Fourier transform infrared spectroscopy

Fourier-transform infrared spectroscopy is derived from the interference of radiation between two beams from the same source. This produces an interferogram which can be transformed using the mathematical method of Fourier-transformation to produce the IR spectrum. Figure 11 displays the main components of an FTIR spectrometer. From the source, the radiation passes through an interferometer and the sample to the detector. This produces a signal which is amplified and then converted to digital form and finally transferred for Fourier-transformation [21].

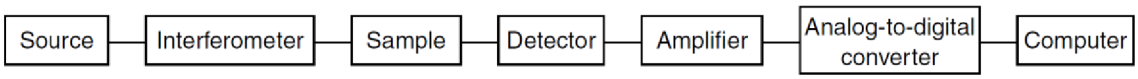

Figure 11: Main components of an FTIR spectrometer [21].

The interferometer consists of two perpendicular plane mirrors and a semi-transparent mirror called *beamsplitter*. One of the plane mirrors is movable, whereas the other one is stationary. The beamsplitter forms an angle of 45° with both mirrors and splits the radiation from the source and sends 50% to the movable mirror and 50% to the stationary mirror. Then the radiation reflects from the plane mirrors to recombine in the beamsplitter to hit the sample. The material of the beamsplitter must be selected according to the region to be studied. This is the Michelson interferometer shown in Figure 12 [21].

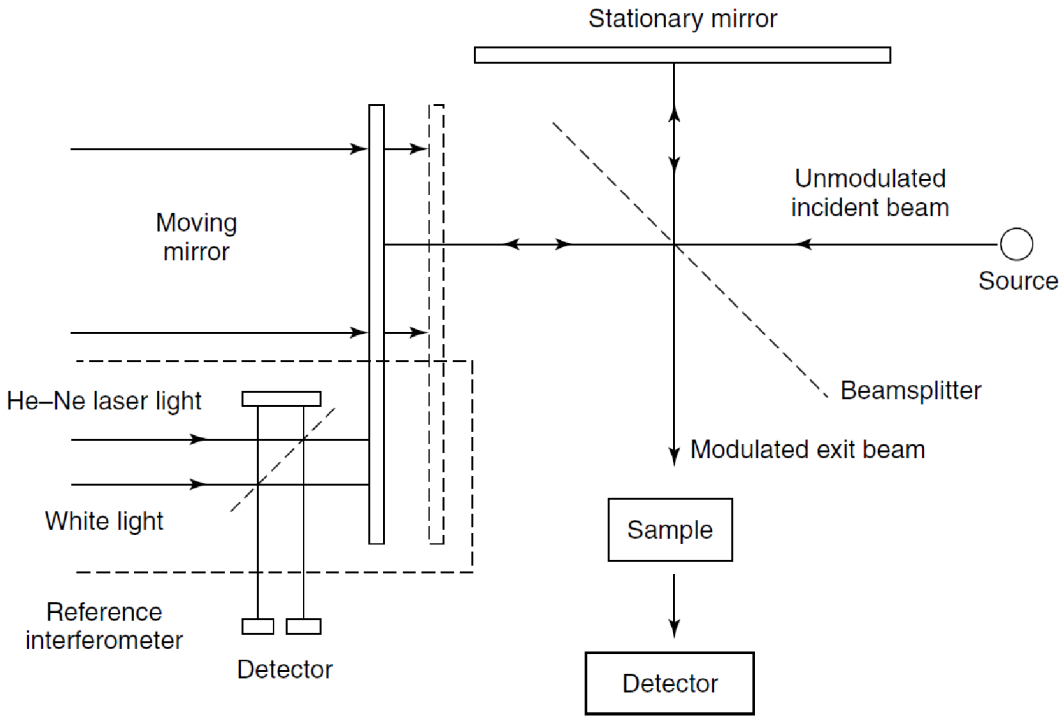

Figure 12: Michelson interferometer schematics [21].

The movable mirror can create a difference in the optical path length between the parts of the interferometer. This results in interference which can be either constructive or destructive. Constructive interference occurs when the path length difference is zero or a multiple of the wavelength of the transmitted radiation. If the optical path difference is non-zero or a multiple of the half-wavelength then the interference is destructive. This interference depends on the frequencies and the position of the moving mirror, every interference pattern relates to one specific wavelength and can be determined from the position of the moving mirror. During measurement, the moving mirror is changing position, and in every position the absorbed light is connected to the positions of the mirror [21].

By using the Fourier-transformation we can convert each interference pattern to specific wavelengths. The two essential equations used for the Fourier-transformation connect the intensity *B(ṽ),* to the spectral power density *I(δ)* at a given wavenumber. The equations are the following:

$$I(\delta) = \int_0^{+\infty} B(\tilde{\upsilon})\cos(2\pi\tilde{\upsilon}\delta)d\tilde{\upsilon}\,, \tag{10}$$

$$B(\tilde{\upsilon}) = \int_{-\infty}^{+\infty} I(\delta)\cos(2\pi\tilde{\upsilon}\delta)d\delta\,, \tag{11}$$

these are interconvertible. “The first shows the variation in power density as a function of the difference in pathlength, which is an interference pattern. The second shows the variation in intensity as a function of wavenumber.” With the Fast Fourier-transformation algorithm we can obtain the infrared spectra [21].

The most used IR radiation sources are the resistively heated silicon carbide rods known as Globar. The standard detector is the deuterated triglycine sulphate (DTGS) detector which uses the pyroelectric effect [20].

There are three main advantages of FTIR spectrometry. One is the improvement of the signal-to-noise ratio (SNR) per unit time. This is the Fellgett advantage and it derives from the many resolution elements being monitored simultaneously. The Jacquinot advantage is caused by the fact that in the FTIR spectrometry the total source output can be passed through the sample. This results in increased energy at the detector. The third is the speed advantage [21].

2.2.3 Infrared spectrum processing

For some use cases, the IR spectrum needs to be manipulated to help both qualitatively and quantitatively better interpret the spectra. There are a few methods for this operation. The first one is the *baseline correction* in which the non-absorbent parts of the IR spectra are joined in a flat line. The next tool is the *smoothing* which helps reduce the noise level. The *difference spectra* are used for subtracting a measured a component from the sample. The fourth one are the *derivatives* which help to find the peak maximum and a lift-off point. The fifth method is the so-called *curve-fitting* which helps find quantitative values for overlapping peaks [21].

In our case, we used a software called IRBAS to subtract the IR spectra of the Si wafer and to remove the thin layer interference effect from the sample. If the substrate is incoherent and non-absorbing, then the transmittance is independent of the substrate thickness. In this case to counter the interference effect, simulated transmittance T_{calc} can be used to subtract from the experimental data. The following equation can be used to calculate the simulated transmittance:

$$T_{calc} = \frac{|\hat{t}_{abc}|^2 |\hat{t}_{ca}|^2}{1-|\hat{r}_{cba}|^2 |\hat{r}_{ca}|^2}, \quad (12)$$

where $\hat{t}_{abc}$ and $\hat{r}_{cba}$ are the complex amplitude reflection and transmission coefficients for the layer b between the media a and c. The complex amplitude reflection and transmission coefficients are dependent on the angle of incidence, the thickness, the extinction coefficient, and the refractive index. Using the refractive index off the three media and film thickness it is possible to construct the T_{calc} for the subtraction [26].

2.2.4 Interpretation of infrared spectra

An infrared spectrum is interpreted using a graph, as shown in Figure 13. The x-axis corresponds to the wavenumber, whereas the y-axis can either depict the transmittance, which can be calculated by:

$$T = \frac{\Phi}{\Phi_0}, \quad (13)$$

where T is the transmittance the Φ is the intensity of the radiation emitted by the source, the Φ_0 is the intensity of the passed radiation, or the absorbance, which can be derived using

$$A = \log \frac{\Phi_0}{\Phi} = -\log T, \quad (14)$$

where A is the absorbance which is equal to the negative logarithm of the transmittance. The two ways of constructing the graph is shown in Figure 13. Using the transmittance is the traditional way, while absorbance is used for quantitative analysis [21,27].

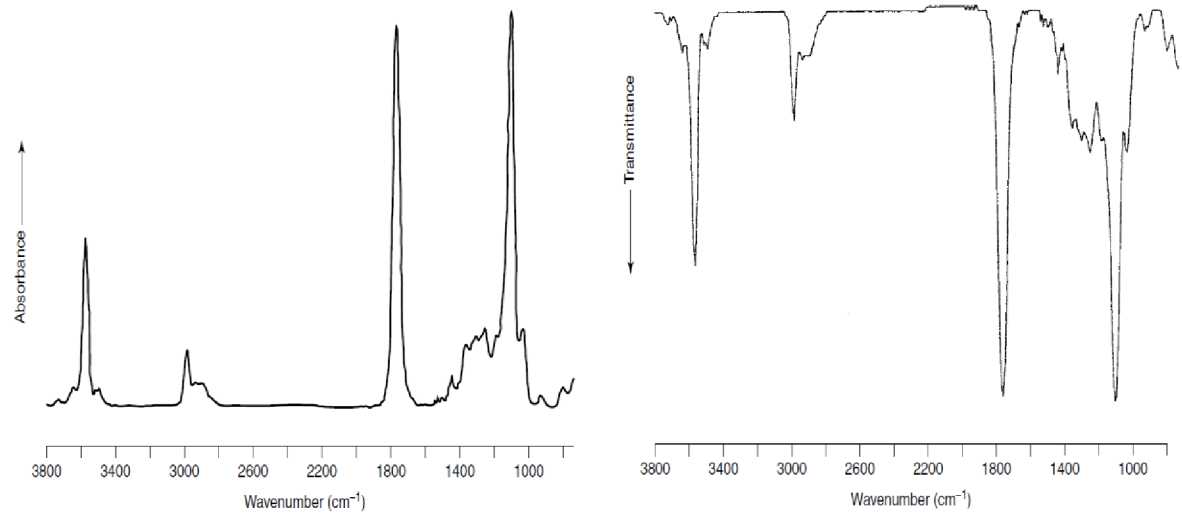

Figure 13: Absorbance and transmittance spectrum of lactic acid [21]

For quantitative analysis, the Beer-Lambert law is used, which relates the absorbance and the concentration according to the equation:

$$A = \varepsilon c l, \tag{15}$$

where A represents the absorbance, c is the concentration, l is the pathlength of the sample and ε is the molar absorptivity [21].

Every peak in the infrared spectra corresponds to one of the characteristic vibrations of bonds in the molecule. In most cases, these peaks are located in the MIR. Vibrations can also interact with each other, which is very common for deformation and group vibrations in the fingerprint region. Using this region, we can easily identify a molecule because it is unique for every molecule. Some of the vibrations are not affected by the other vibrations and are used for identifying functional groups. It is possible to create a database of organic molecule IR spectra. Based on these laws, we can compare the unknown molecules spectrum to the one which is found in the database. We can also assign some of the bonds to the peaks using tables and diagrams shown in Table 2 [21].

Table 2: Infrared characteristic frequencies of specific organosilicon compounds [28].

Specific bonds	Wavenumber (cm^{-1})
H-SiR_3	2110-2094
H-SiR_2Ar	2115-2103
H-$SiAr_3$	2132-2112
Si-CH_2-R	1250-1200
Si-CH_3	1280-1255
Si-OCH_3	1110-1107
Si-OH	920-830
Si-O-Si	1100-1000

3 EXPERIMENTAL PART

3.1 Materials

The monomer used for the thin film preparation is tetravinylsilane (TVS) provided by Sigma-Aldrich. The structure of the monomer is shown in Figure 14, and its main properties are displayed in Table 3. The TVS is stored in a glass vessel at a pressure of 800 Pa and it is cooled with water to the temperature of 14,9 °C. The temperature of the monomer is maintained using a Circulating thermostat PT31 made by the company A. Krüss Optronic GmbH. Figure 15 shows the container and the cooling system of the monomer. In the glass vessel, the monomer is in its liquid state with its vapours over it. For the deposition, the monomer is used in its gas phase.

Table 3: Properties of the TVS

Name	Tetravinylsilane
Formula	$C_8H_{12}Si$
Molecular weight	136,27 $g \cdot mol^{-1}$
Boiling point	130-131 °C
Density	0,8 $g \cdot cm^{-3}$
Reflective index	1,461
Purity	97 %

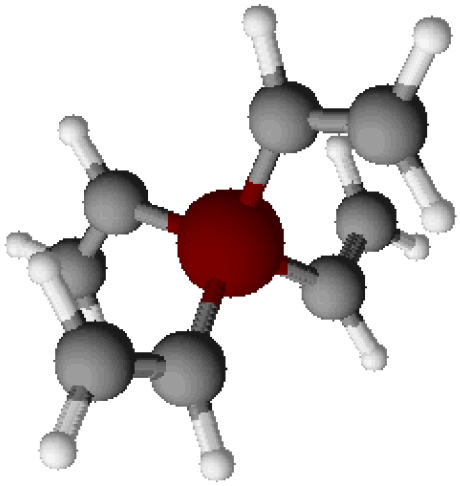

Figure 14: The 3D structure of the tetravinylsilane.

Figure 15: (A) the glass container of the monomer (B) the thermostat.

The substrate on which the thin film is deposited is a silicon wafer with its two sides polished and covered with a native oxide layer supplied by the company ON Semiconductor Czech Republic. Its dimensions are 10 × 10 × 0,6 mm. Before the deposition, the wafer is cleaned using an ultrasonic bath in ethanol for 15 minutes and then in water, again for 15 minutes. Then it is left for one day to dry. Only the perfectly cleaned wafers, without any dust on them, are used. The wafers are stored in plastic boxes inside a desiccator. The silicon wafer is shown in Figure 16.

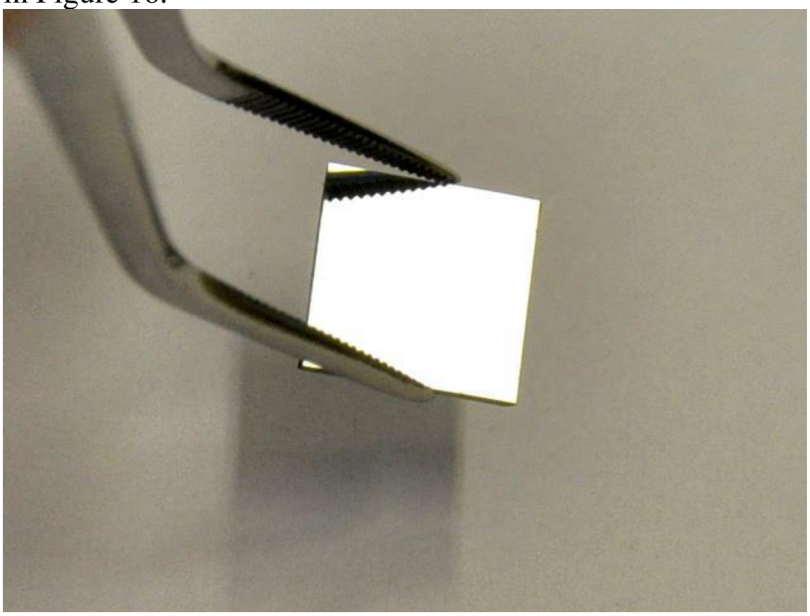

Figure 16: Cleaned silicon wafer

3.2 Deposition system

The plasma enhanced chemical vapour deposition is carried out inside a high-vacuum system called A3, the scheme of the apparatus is shown in Figure 17. The A3 system is constructed to maintain a vacuum at 10^{-6} Pa and capacitively coupled plasma. All parts of the vacuum apparatus are made of stainless steel (AISI 304, 321) supplied by Vakuum Praha, which are connected by a copper vacuum seal or vacuum "O-rings" made of fluorinated rubber. A system of two pumps is used to create a high vacuum. The first in the pumping system is a scroll vacuum pump, which establishes the fore vacuum. This is a TriScroll 300 pump made by the company Varian, with a pumping speed of 210 l/min, enabling pressures in the range of 1 – 10Pa units to be achieved. The TMU 261P turbomolecular pump made by Pfeiffer Vacuum, with a pumping speed of 170 l/s, is used to obtain a high vacuum in the reactor space. This turbomolecular pump cannot have a pressure higher than 100 Pa at its inlet or outlet, therefore the aforementioned scroll vacuum pump is used to create the fore vacuum.

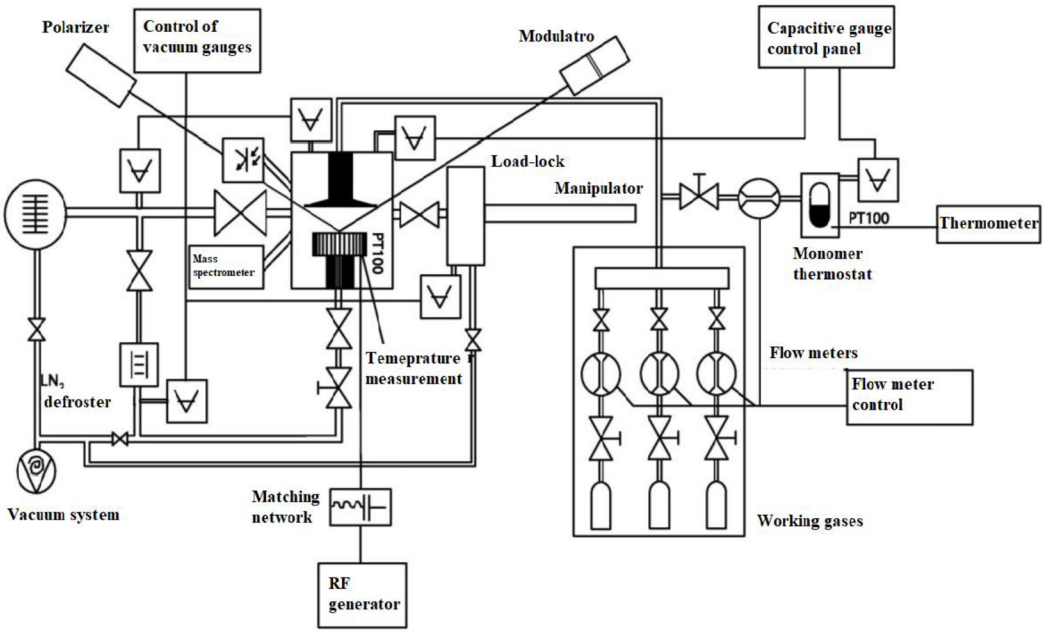

Figure 17: A3 apparatus scheme.

The main part of the apparatus consists of a cylindrical reactor chamber, measuring 25 × 25 cm. Inside the reactor, there are two plane-parallel copper Oxygen Free High Conductivity (OFHC) electrodes with a diameter of 114 mm. The upper electrode is grounded, and gases are fed through it to the reactor. The lower is the working rotating electrode, it is supplied with radiofrequency power (13.56 MHz) and can hold up to six samples. The plasma is generated by the RF generator (Caesar 1310 from Advanced Energy Company). The generator can be used either in a pulsing mode or in a continual mode. To define power in the pulsing mode, we use a variable called Effective power (P_{eff}), which is defined by the equation:

$$P_{eff} = \frac{t_{on}}{t_{on}+t_{off}} \cdot P, \tag{16}$$

where t_{on} is the time when the generator supplies power, t_{off} is the time when the generator is not suppling power and P is the nominal power.

An LC matching network (VM1000 Digital matching network from Advanced energy) is used to handle the reflected power, which is caused by the impedance mismatch in the RF circuit. The samples are mounted in holders shown in Figure 18, also made of OFHC copper, and are inserted into the electrode from the separation chamber, called load-lock by a magnetic manipulator. An in-situ phase-modulated spectroscopic ellipsometer (UVISEL, made by HORIBA Scientific) is connected to the deposition apparatus to examine the optical properties of the samples and to measure the thickness and the growth rate of the polymer layer during deposition. Furthermore, a mass spectrometer (Process Gas Analyser HPR-30 made by Hiden Analytical) is connected to the reactor to measure the purity of the system and to examine the reaction processes during deposition.

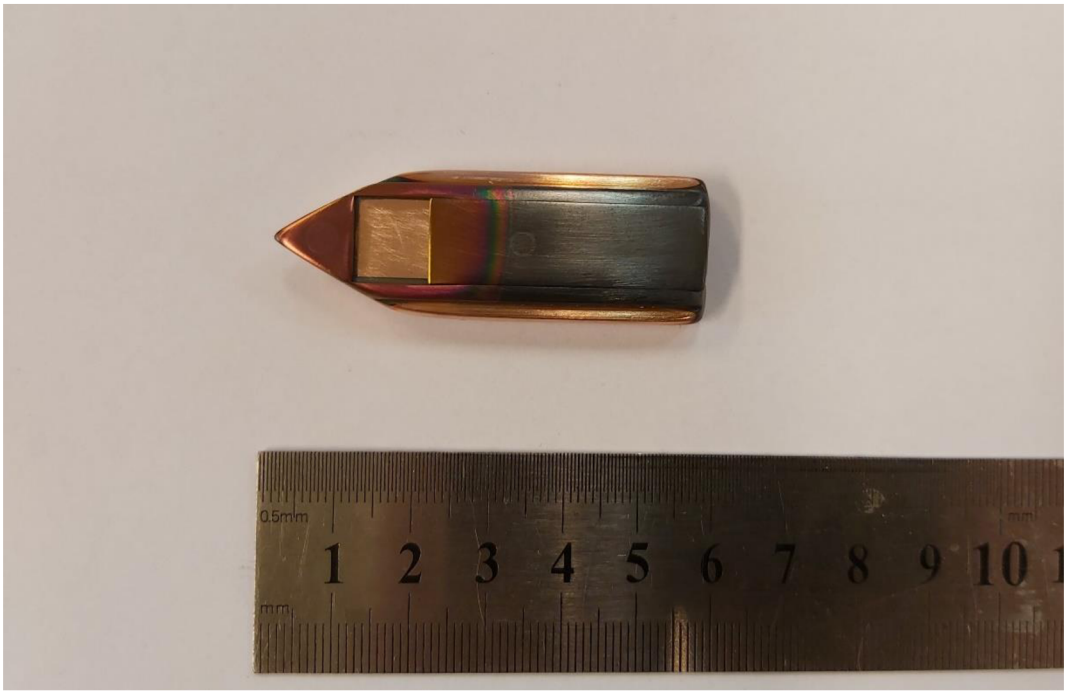

Figure 18: Sample holder after the deposition.

The deposition system is controlled by the A3 controller software, this is shown in Figure 19. This program can control and monitor every aspect of the deposition, such as the gas flow, the power supplied to the electrodes, the matching network. It also controls the vacuum system, the opening, and closing of the valves and monitors the pressures in the individual parts of the apparatus. The A3 controller program communicates via the RS-232 interface.

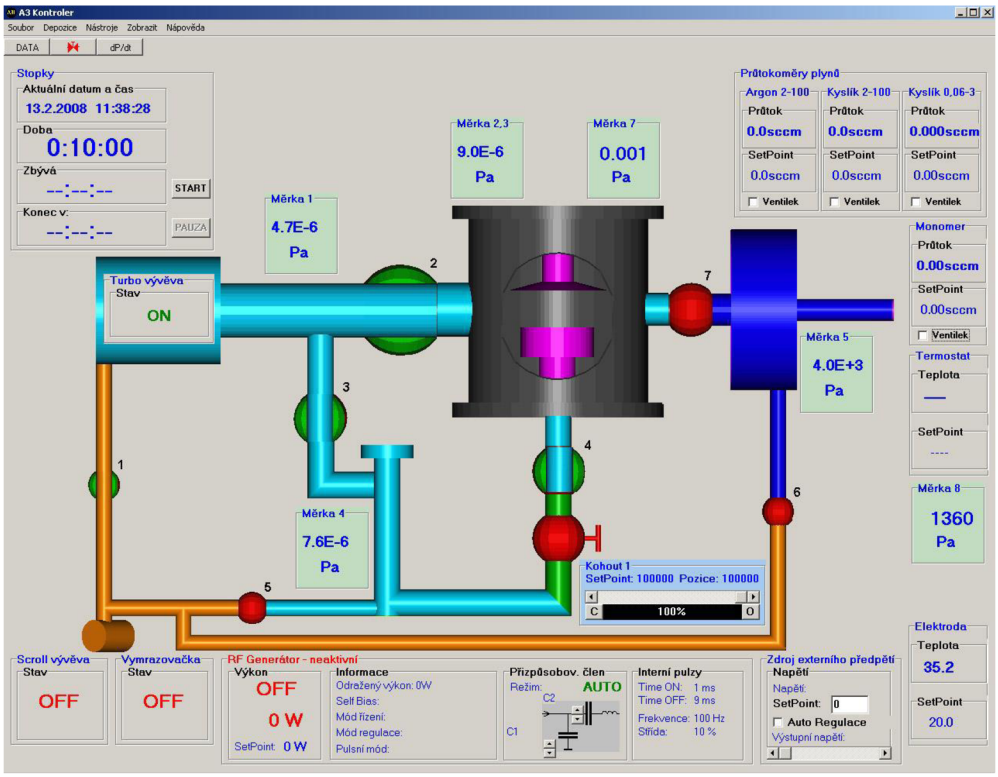

Figure 19: A3 controller program

3.3 Deposition steps and conditions.

The following steps describe the sample preparation process. This process assumes an evacuated chamber.

- The first step is to load the cleaned silicon wafers into the cleaned sample holders.
- The next step is to vent the load-lock and load the samples into the carousel inside the load-lock and take out the previously created samples. The load-lock is vented for a short time with dry air to prevent contamination of the reactor chamber and to shorten the pumping time. Also, the samples are rinsed with air to remove any dust on their surface.
- The next step is the evacuation of the load-lock and putting the samples inside the reaction chamber. The evacuation is carried out by closing valve 1 and opening valve 6. When the pressure is satisfying adequate valve 6 is closed and valve 1 and 7 are opened. Afterwards, the sample holders are moved from the load-lock to the reaction chamber with the magnetic linear drive manipulator. The sample tray inside the reaction chamber must be balanced, for this propose sometimes a blank wafer is used.
- When the samples are inside the chamber valve 7 is closed and valve 2 is opened, the chamber is evacuated to the range of pressure 10^{-5} Pa. Then the monomer path is vented from the leftover TVS. Also, an ellipsometry is carried out to measure the thickness of the SiO_2 film on the surface of the silicon wafer.
- In this step, the surface of the samples is cleaned and activated with argon plasma pre-treatment. Valve 2 is closed, and the Ar gas flow rate is set to 10 sccm (standard cubic centimeters per minute), and pressure is set to 5,7 Pa by changing the position of the butterfly valve. After the pressure reaches 5,7 Pa and is constant the RF generator is

turned on at 5 W power in a continual mode for 10 min, the matching network is set to C_1 = 79,0 %; C_2 = 34,2 %.

- After this step, the generator is turned off and Ar flow is set to 0 sccm. Valve 2 is opened, and the chamber is evacuated for 10 min to the range of pressure 10^{-5} Pa. During the evacuation the shutter is placed above the samples.
- The next step is the deposition process. Valve 2 is closed, and TVS gas flow is set to 29 sccm (N2) and the butterfly valve is set to maintain the pressure at 2,7 Pa. If the pressure is constant the generator is turned on in a required power and mode, and the matching network is set to minimize the reflective power. Table 4 shows the settings for the examined thin films. After the generator is set to the required power, the shutter is moved away, and a timer is started. At this point, the deposition begins, and the matching network settings are changed again to get 0 reflective power. The generator is turned off after the required time has passed for the required thickness. During the deposition, data is collected from every aspect of the deposition conditions in an excel file.
- After this step, the TVS gas flow is turned off and after the pressure is under 2 Pa valve 2 and 8 are opened and the reactor is evacuated for 10 min. During this step, the film thickness and optical properties are measured using spectroscopic ellipsometry.
- The next step is the argon posttreatment to reduce the presence of free radicals in the chamber and on the surface of the film. Valve 2 is closed and Ar flow is set to 10 sccm at a pressure of 5,7 Pa for 1 hour.
- In the last step, the Ar flow is stopped and valve 2 and 8 are opened to create sufficient vacuum in the chamber and after that, the chamber is prepared for a new deposition.

Table 4: Deposition conditions of the examined thin films and the final thickness.

Series designation	Sample number	RF Power setting				Gas flow rates	Pressure	Thickness
		P_{eff} [w]	P [w]	t_{on} [ms]	t_{off} [ms]	TVS [sccm]	P_7 [Pa]	[nm]
TVS only	A3804	2	10	1	4	29	2,7	707,237
	A3805	10	50	1	4	29	2,7	581,115
	A3808	25	200	1	7	29	2,7	653,053
	A3809	75	300	1	3	29	2,7	584,163
	A3854	150	300	1	1	29	2,7	729,570

Thin films can also be prepared by adding O_2 or Ar to the gas mixture during the deposition, but in this thesis, we are only examining pure TVS samples. In Table 4 the gas flow of the monomer is set to 29 sccm because the flowmeter is calibrated to measure the flow of N_2. The real flow of the monomer is 3,87 sccm.

3.4 Instrumentation of the infrared spectroscopy

The prepared thin films were analysed with FTIR spectroscopy to determine the chemical structure of the films. The used instrument was Vertex 80v manufactured by the Bruker Corporation.

VERTEX 80v is a vacuum FTIR spectrometer with an UltraScan^{TM} interferometer providing high spectral resolution. Good stability and measurement sensitivity are ensured by a linear air bearing, precise adjustment of the interferometer's scanning arm, and high-quality optics. TrueAlignment^{TM} technology prevents false peaks and noise. The device allows measuring in the middle, near and far IR region, without masking very weak spectral information due to the absorption of water vapor or CO_2. In the standard configuration of the device, a resolution of about 0,2 cm^{-1} is achieved. Figure 20 shows the Vertex 80v and its components. All functions of the VERTEX 80v are controlled using the OPUS software [29].

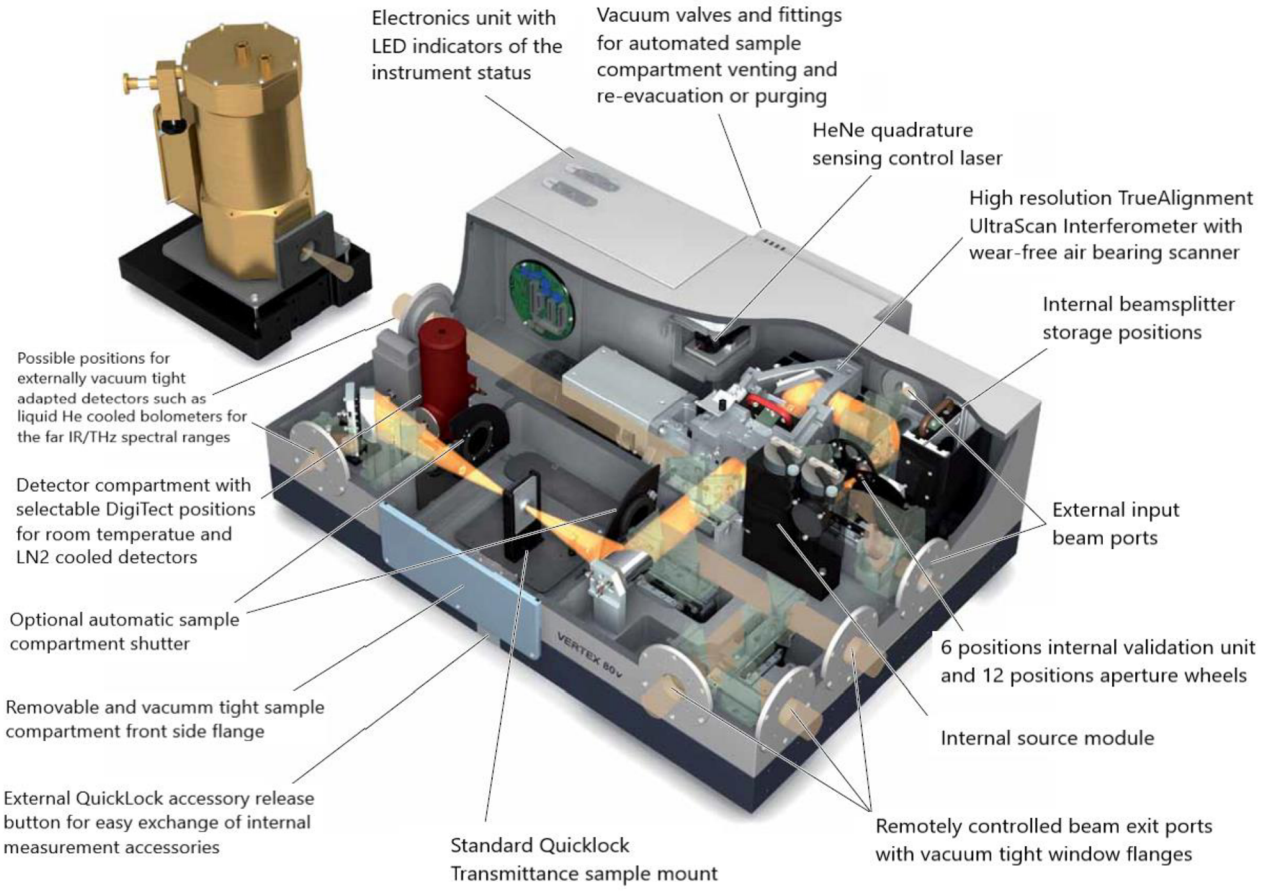

Figure 20: Vertex 80v and components [29].

3.5 Measurement and correction of infrared spectra

The samples displayed in Table 4 were provided to me for the measurement. The following steps show how the infrared spectra are obtained and after that how it was processed. The processing is needed to make the infrared spectra readable and comparable with other IR spectra.

- The first step is the evacuation of the sample chamber and the beam path. This is important to reduce the presence of H_2O and CO_2 molecules and any other gases which absorb in IR wavelength. The sufficient level of vacuum is around 120 Pa.
- The next step is to set the parameters of the measurement. The scale is from 4 000 – 400 cm^{-1}, the resolution is set to 4 cm^{-1} and there are 256 scans for the background and each sample.
- In the following step, the background is measured, and the sample chamber is vented. Then the sample is placed inside the chamber and it is again evacuated at least for 1 hour.
- After the sufficient vacuum is reached the sample is measured. The OPUS software then subtracts the background measurement. After this, the chamber is vented, and the next sample is placed inside.
- After the measurement, the raw data is saved for further processing.
- In this step, the IRBAS program is used to eliminate the absorption of the silicon substrate and to correct the baseline for countering the interference effect of the samples. Because the samples have different thicknesses the IRBAS program normalises them to the absorption of 1 000 nm thick film. This is needed to make the spectra accurately comparable. Figure 21 shows the IRBAS software.
- Then in the ORIGIN software, the IR spectra get their final form by using further baseline correction and by forming them into readable graphs.

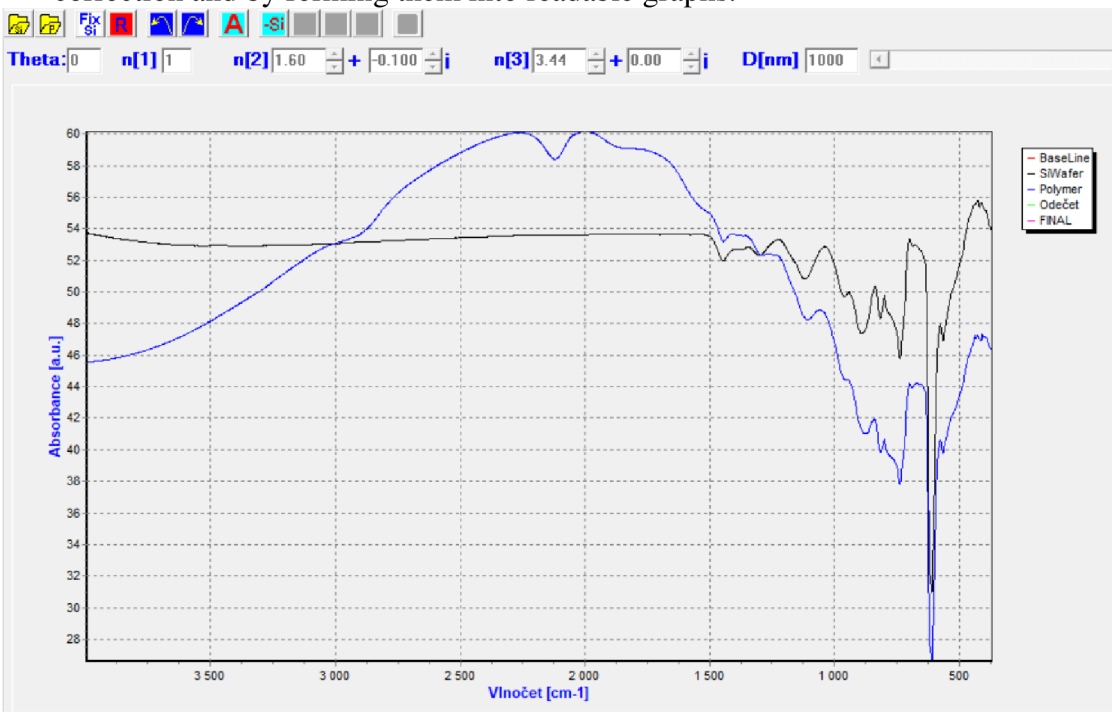

Figure 21: The subtraction of Si absorption in the IRBAS software.

4 RESULTS AND DISCUSSION

4.1 Processing of the infrared spectra

In the first part of the results and discussion section, it is important to show how the modifications are changing the raw data from the FTIR spectroscope. Figure 22 shows the changes in the spectra of the 2 W sample. The light green curve shows the raw data from the spectroscope after the background subtraction. After this, by looking at the blue curve, we can observe how some peaks are reduced or eliminated by the Si wafer subtraction. The red curve shows the changes resulting from the interference countering. The final form is represented by the dark green curve and in this step, we can see the least changes.

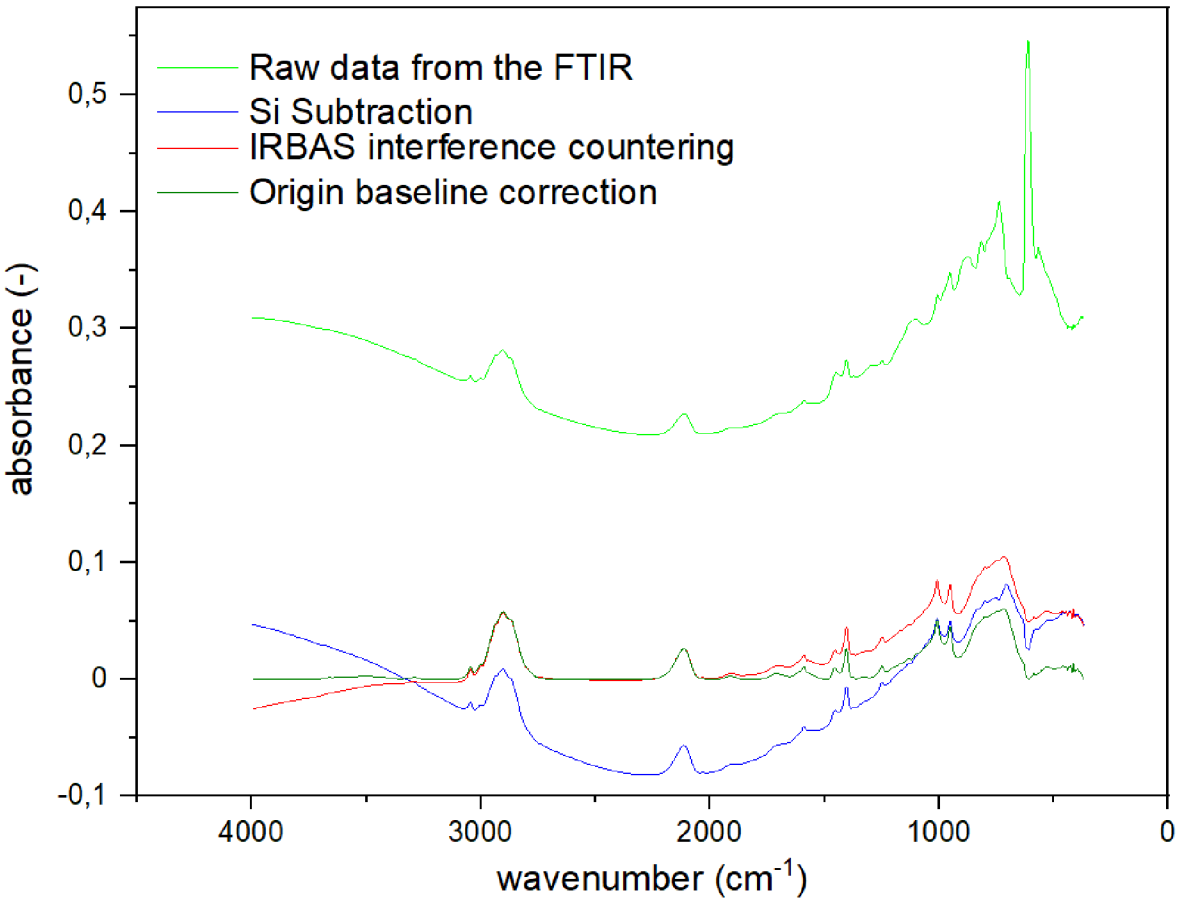

Figure 22: Changes to the IR spectra of the 2°W sample.

After these modifications, the infrared spectra of the five samples are displayed in one graph to identify and compare the absorption in selected wavenumbers, as shown in Figure 23.

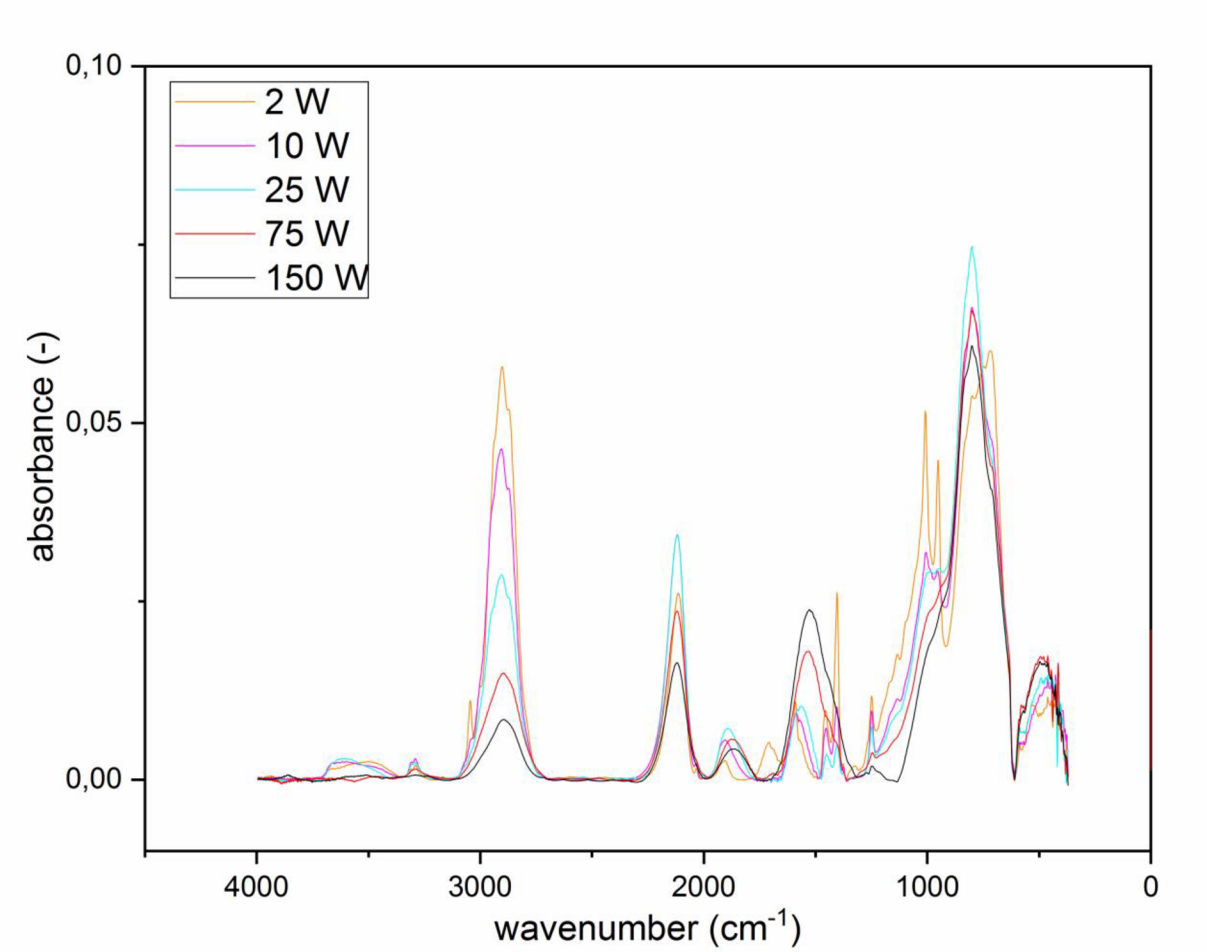

Figure 23: The final form of the IR spectra of the measured samples displayed in one graph.

4.2 Determination of the chemical structure from the infrared spectra

From the infrared spectra of the deposited samples, I identified 14 different peaks. Some of these peaks help us understand how the chemical structure changes when changing the effective power of the deposition. In Figure 24 we can see the identified peaks and in Table 5 we can find the description, the details, and the references of the peaks. We know that when a peak area is changing it means that the number of bonds corresponding for that peak is also changing and these are directly proportional. Since the IRBAS software normalized the thickness of the samples to 1000 nm, we don't have to take into account the different thicknesses of the samples.

The first identified peak is O-H stretching at a range of 3 676 – 3 415 cm^{-1}. This peak is present in the samples of 2 – 25 W. The peak is present due to the oxidation of the Si-H bond in the samples [30,31]. The OH group is not present in the samples 75 – 150 W due to lower number of Si-H bonds in the samples and the crosslinking influence of the reaction kinetics [32]. The next peak is C≡C-H stretching at 3 290 cm^{-1}, this group is not present in the monomer and it is created during the dissociation of the monomer by the plasma in the PECVD process [33,34].

The third absorption band is CH_x stretching (x=1, 2, 3) at 2 2903 cm^{-1}, in this band we can identify 5 different peaks, these peaks can be assigned to the number of a hydrogen atom bonded to the C atoms and the bond hybridization on the C atom [35]. This peak shows a trend: by increasing the effective power of the deposition the absorption band intensity is decreasing. This means that during the deposition by increasing the effective power there is a higher dissociation of the monomer and more H atoms are eliminated and thus new bonds are created. By this effect we assume that the crosslinking is increasing by the increment of the effective power [36]. The changes in the CH_x group are shown in Figure 25.

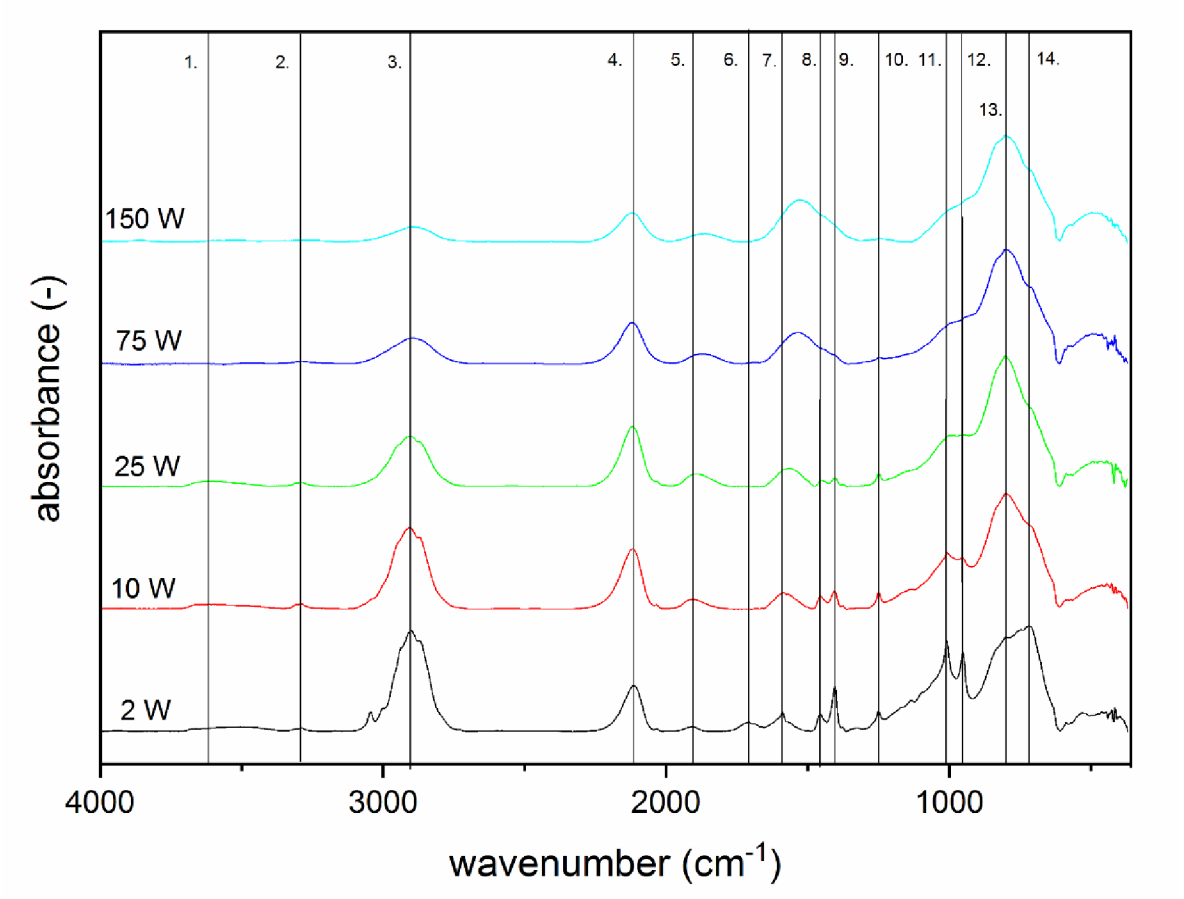

Figure 24: The identified peaks in the IR spectra of the measured samples.

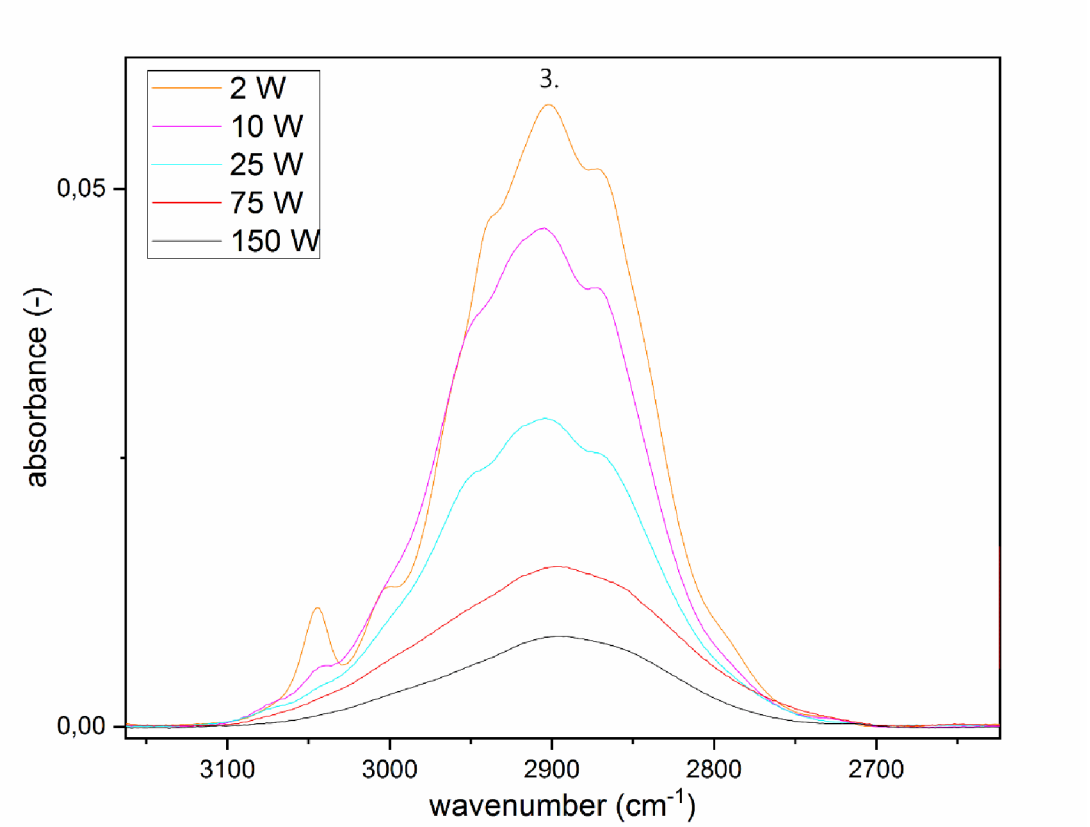

Figure 25: Absorption of the CH_x group in the examined samples.

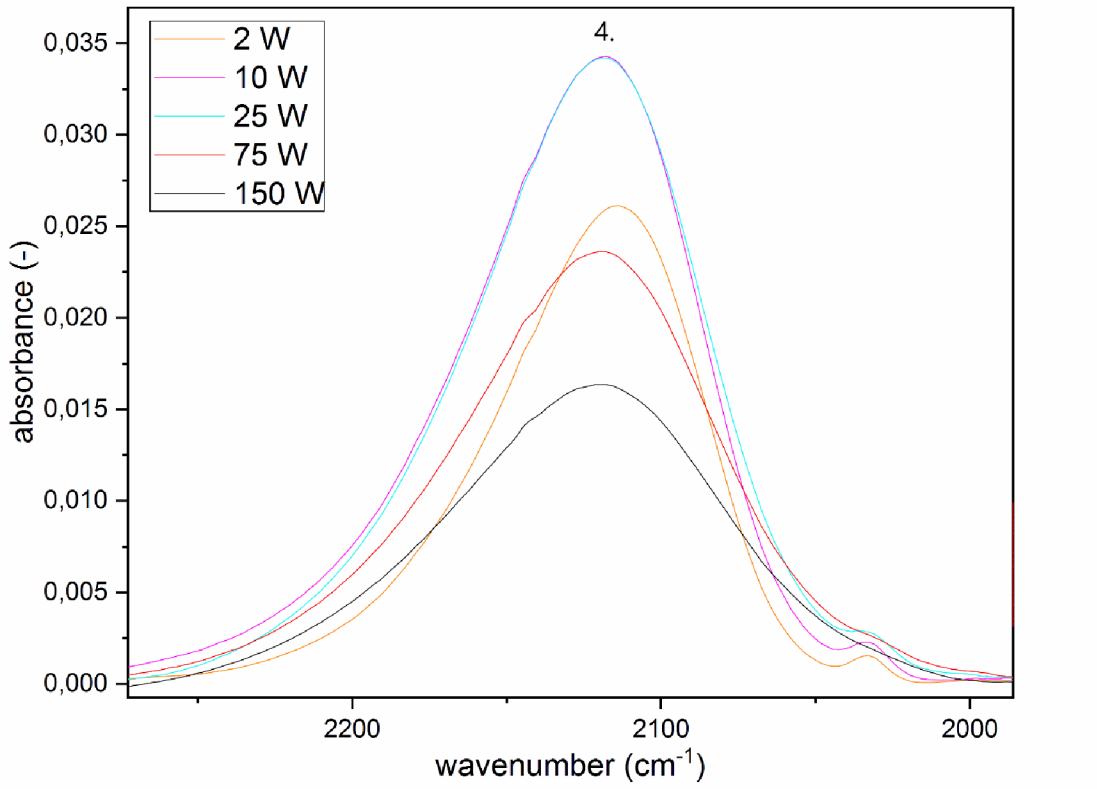

Figure 26: Changes in Si-H stretching in the measured samples.

The fourth assigned peak is Si-H stretching at 2 116 cm^{-1}. The intensity of this peak is increasing in the samples 2 – 25 W and decreasing in samples 75 – 150 W. This peak is shown in Figure 26.

The fifth peak is at 1 907 – 1 872 cm^{-1}, its intensity does not really change by changing the effective power. The identification of this absorption band is very challenging because I could not find clear evidence for this peak in the previous measurement of these thin films. However, I assume this peak corresponds to the C=C=C stretching because the wavenumber of this band in the sample corresponds with this absorption [28] and the group is created during the deposition, which we know from previous mass spectrometry measurement [33]. The six assigned peak is C=O stretching at 1 711 cm^{-1}, this peak is created after the deposition by oxidation of the CH_x group. Because the CH_x group is reduced in the samples created with higher effective power and the reaction kinetics is influenced with the higher crosslinking the C=O band is appearing only in the 2 W sample [32]. The seventh assigned peak is C=C stretching at 1 591 – 1 525 cm^{-1}, the intensity of this peak is increasing with the increment of the effective power of the deposition. This peaks increase provides evidence for the increase of the sp^2 hybridization [37]. Peak 8 is CH_2 scissoring at 1 456 cm^{-1} and peak 9 is CH_2 deformation in the vinyl group at 1 406 cm^{-1}. The change in the peaks 5^{th} – 9^{th} is shown in Figure 27.

The tenth assigned peak is CH_2 wagging in the Si-CH_2-R group at 1 250 cm^{-1}, the eleventh peak is assigned to =CH wagging in the vinyl group at 1 011 cm^{-1}, the twelfth peak is =CH_2 wagging in the vinyl group at 953 cm^{-1}. The peaks 8^{th}, 9^{th}, 11^{th} and 12^{th} these peaks intensity is decreasing with the enhancement of the effective power, but the C=C stretching is increasing, this is also evidence for the increase of the crosslinking in the samples [37]. The thirteenth peak is assigned to Si-H bending at 797 cm^{-1}, we can observe a similar effect in the changes of the intensity like in the case of the fourth peak because these two absorption bands are corresponding for the same bond in the sample. The fourteenth peak is Si-C stretching at 719 cm^{-1} this peaks intensity is also decreasing by the increment of the effective power in the deposition. In the case of the 4^{th}, 10^{th}, 13^{th} and 14^{th} peaks the decrease of the peak intensity is the result of the increasing of the C/Si ratio and the decrease of the Si concentration with the increasing effective power in the deposition [38]. The peaks 10^{th} – 14^{th} are shown in Figure 28.

In the case of C=C=C stretching in the 5^{th} peak and C=C stretching in the 7^{th} peak we can observe a peak shifting to the lower wavenumbers and a peak base broadening in the 75 – 150 W samples. This effect is caused by the chemical structural changes in the samples which are affecting these bonds [39].

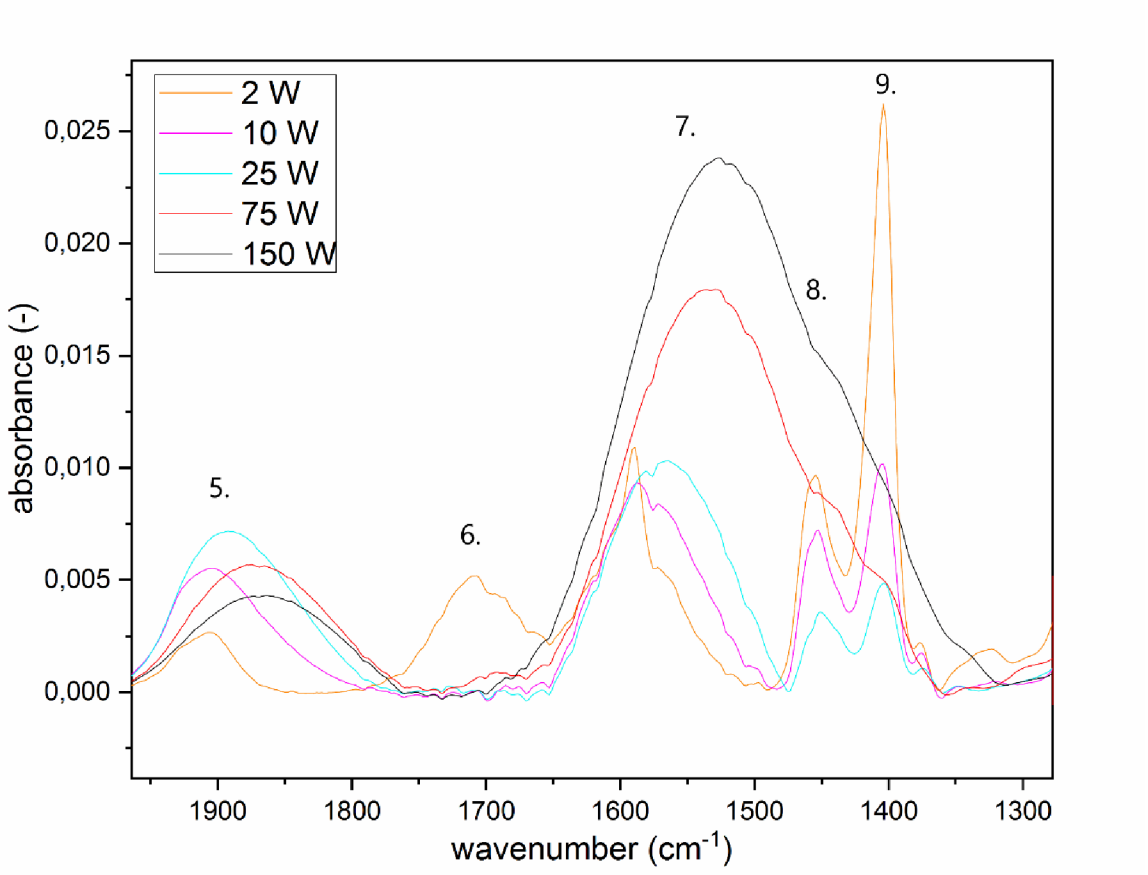

Figure 27: Changes in the intensity of the 5th – 9th assigned peaks in the samples.

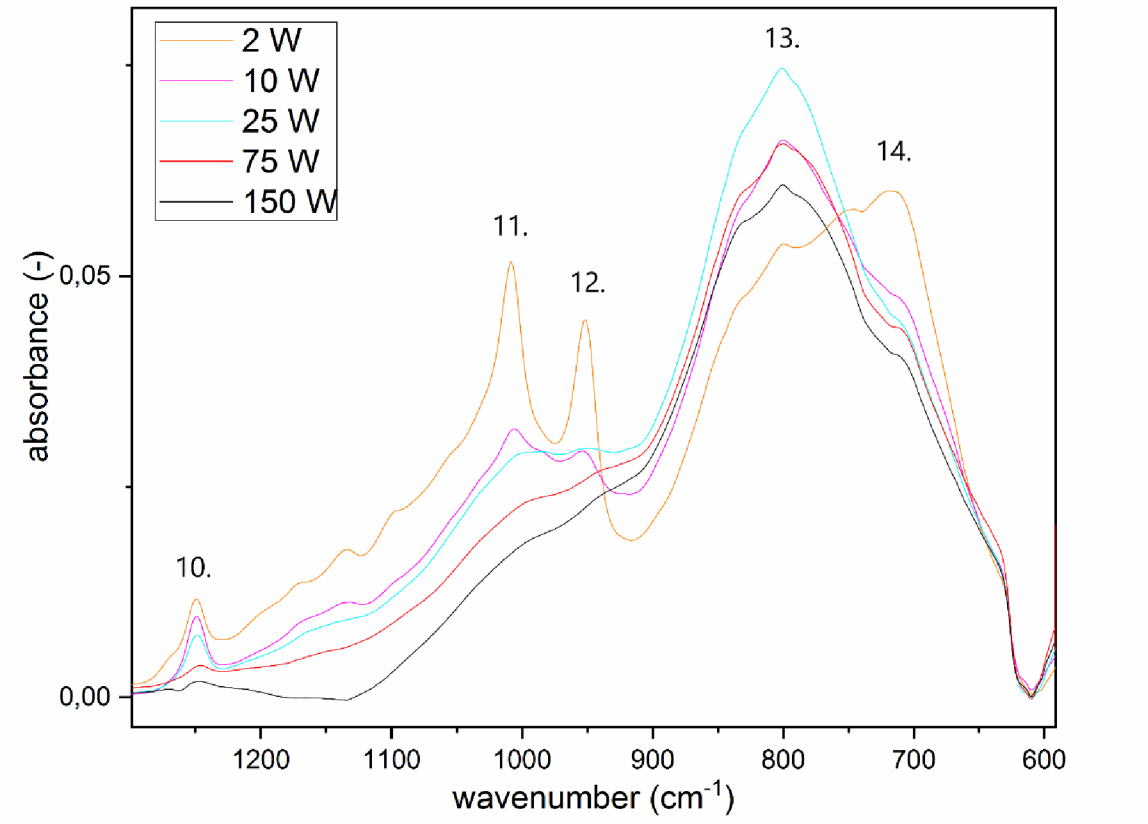

Figure 28. Changes in the intensity of the 10th – 14th assigned peaks in the samples.

Table 5: Assigned peaks in the measured IR spectra.

Peak numbers	Wavenumber (cm^{-1})	Assignment	Peak range from the reference (cm^{-1})	Reference
1.	3 679 – 3 415	O-H stretching	3 700 – 3 200	[28,30-32,40]
2.	3 290	C≡C-H stretching	3 340 – 3 270	[28]
3.	2 903	CH_x stretching (x=1, 2, 3)	3 100 – 2 750	[28,35,36,41]
4.	2 116	Si-H stretching	2 320 – 2 00	[28,35,38]
5.	1 907 – 1 872	C=C=C stretching	2 000 – 1 900	[28]
6.	1 711	C=O stretching	1 710 – 1 660	[28,32]
7.	1 591 – 1 525	C=C stretching in vinyl group	1 620 – 1 500	[28,37,40]
8.	1 456	CH_2 scissoring	1 475 – 1 420	[28,40]
9.	1 406	CH_2 deformation in vinyl group	1 430 – 1 390	[28,40]
10.	1 250	CH_2 wagging in Si-CH_2-R	1 260 – 1 200	[28,38,40]
11.	1 011	=CH wagging	1 020 – 1 000	[28,40]
12.	953	$=CH_2$ wagging	980 – 950	[28,40]
13.	797	Si-H bending	845 – 800	[28,35,40]
14.	719	Si-C stretching	760 – 680	[28,40]

5 CONCLUSION

In this Bachelor thesis 5 samples of thin films deposited on silicon wafers using tetravinylsilane were examined. The examined samples were deposited with different effective power from 2 W to 150 W. The main objects of this analysis were the chemical structure of these thin films and its changes with the different power.

A Fourier transform infrared spectrometer was used for the determination of the chemical structure. After the processing of the raw data the transmission infrared spectre were obtained. Fourteen different absorption peaks were identified in the spectrum. The peaks were assigned to the vibrations of specific chemical species. The changes in these peaks were closely examined and compared with previous results in this field, to find a cause in the changes throughout the samples.

The following species are present in the deposited thin films: CH_x groups, Si-C and Si-H, sp^1, sp^2 and sp^3 hybridizations on the carbon atoms in the sample manifested in C≡C and C=C species, also there is oxygen atoms present in the samples caused by the oxidation process in the air.

During the deposition process the tetravinylsilane molecule is fragmented and creates carbon-silicon network from the mentioned atoms and bonds. The decreased CH_x groups with enhance power and the decreased peaks with hydrogen atom present, provide evidence for the chemical structure becomes more crosslinked with the enhanced effective power. This means that with the increase in crosslinking the number of hydrogen atoms are decreased and the number of C-C and C=C bonds are increased. The decrease of the Si-C species provides evidence for the decrease in C/Si ratio. Also, the lack of the O-H and C=O groups presence in the samples 75 W and 150 W provides evidence for the increase of network crosslinking.

In a future research we can examine samples deposited with different monomers. Samples will be deposited using monomers without double bonds and the presence C=C double bonds created during the deposition will be examined. Also, we can further examine the oxidation effect on these layers.

6 REFERENCES

[1] FREUND, L.B and S. SURESH. *Thin film materials: stress, defect formation and surface evolution*. Cambridge: Cambridge University Press, 2003. ISBN 0-521-82281-5.

[2] OHRING, Milton. *Materials science of thin films: deposition and structure*. 2nd ed. San Diego: Academic Press, 2002. ISBN 0-12-524975-6.

[3] WASA, Kiyotaka, Hideaki ADACHI and Makoto KITABATAKE. *Thin film materials technology: sputtering of compound materials*. Norwich: William Andrew Publishing, c2004. ISBN 0-8155-1483-2.

[4] SZALAY, Béla. *Fizika*. 6th edition. Budapest: Műszaki Könyvkiadó, 1979. ISBN 963-10-2661-2.

[5] ECKERTOVÁ, Ludmila. *Physics of thin films*. New York: Plenum Press, 1977.

[6] HOFFMAN, Dorothy M., Bawa SINGH and John H. THOMAS. *Handbook of vacuum science and technology*. San Diego, CA: Academic Press, c1998. ISBN 01-235-2065-7.

[7] INAGAKI, N. *Plasma surface modification and plasma polymerization*. Lancaster, Pa.: Technomic Pub. Co., c1996. ISBN 1566763371.

[8] MARTIŠOVITŠ, Viktor. *Základy fyziky plazmy: učebný text pre magisterské štúdium*. Bratislava: Vydavateľstvo UK, 2006. ISBN 80-223-1983-X.

[9] BITTENCOURT, J. A. *Fundamentals of plasma physics*. 3rd ed. New York: Springer, c2004. ISBN 0387209751.

[10] YASUDA, H. *Plasma polymerization*. Orlando: Academic Press, 1985. ISBN 0127687602.

[11] WROBEL, A. M, and M. R. WERTHEIMER. Plasma-polymerized organosilicones and organometallics. in D'AGOSTINO, R. *Plasma Deposition, Treatment and Etching of Polymers*. San Diego, CA: Academic Press, 1990, s. 163-220. ISBN 0-12-200430-2.

[12] ZANINI, Stefano, Claudia RICCARDI, Marco ORLANDI and Elisa GRIMOLDI. Characterisation of SiOxCyHz thin films deposited by low-temperature PECVD. *Vacuum* [online]. 2007, **82**(2), 290-293 [cit. 2020-07-21]. DOI: 10.1016/j.vacuum.2007.07.001. ISSN 0042207X. Available from: https://linkinghub.elsevier.com/retrieve/pii/S0042207X07002084

[13] COCLITE, Anna Maria, Antonella MILELLA, Riccardo D'AGOSTINO and Fabio PALUMBO. On the relationship between the structure and the barrier performance of plasma deposited silicon dioxide-like films. *Surface and Coatings Technology* [online]. 2010, vol. 204, issue 24, s. 4012-4017 [cit. 2020-07-21]. DOI: 10.1016/j.surfcoat.2010.05.024. Available from: http://linkinghub.elsevier.com/retrieve/pii/S0257897210003853

[14] MACKOVA, A., V. PERINA, Z. STRYHAL, J. PAVLIK, M. SVEC, A. QUEDE, P. SUPIOT, G. BORVON, A. GRANIER and P. RAYNAUD. The combined study of the organosilicon films by RBS, ERDA and AFM analytical methods obtained from PECVD and PACVD. *Surface Science* [online]. 2004, vol. 566-568, s. 1143-1146 [cit. 2020-07-21]. DOI: 10.1016/j.susc.2004.06.072. Available from: http://linkinghub.elsevier.com/retrieve/pii/S0039602804007411

[15] YI, Jeong W, Young H LEE and Bakhtier FAROUK. Effects of gas composition and r.f. power on properties of a–C:H/SiC:H composite films grown by plasma-enhanced chemical vapor deposition. *Thin Solid Films* [online]. 1998, vol. 326, issue 1-2, s. 154-159 [cit. 2020-07-21]. DOI: 10.1016/s0040-6090(98)00565-3. Available from: http://linkinghub.elsevier.com/retrieve/pii/S0040609098005653

[16] ČECH, V., J. STUDÝNKA, N. CONTE and V. PEŘINA. Physico-chemical properties of plasma-polymerized tetravinylsilane. *Surface & Coatings Technology*. 2007, (201), 5512-5517. ISSN 0257-8972.

[17] PARK, Jaebeom, Jongsik OH, Elly GIL and Geun Young YEOM. Characteristics of SiOX thin films deposited by atmospheric pressure chemical vapor deposition using a doubledischarge system. *Materials Research Bulletin* [online]. 2012, vol. 47, issue 10, s. 3011-3014 [cit. 2020-07-21]. DOI: 10.1016/j.materresbull.2012.04.124. Available from: http://linkinghub.elsevier.com/retrieve/pii/S0025540812003285

[18] RAU, Christiane and Wilhelm KULISCH. Mechanisms of plasma polymerization of various silico-organic monomers. *Thin Solid Films* [online]. 1994, vol. 249, issue 1, s. 28-37 [cit. 2020-07-21]. DOI: 10.1016/0040-6090(94)90081-7. Available from: http://linkinghub.elsevier.com/retrieve/pii/0040609094900817

[19] *Handbook of deposition technologies for films and coatings: science, applications and technology*. Third edition. Editor Peter M. MARTIN. Amsterdam: Elsevier, [2010]. ISBN 978-0-8155-2031-3.

[20] GAILITZ, G. and Tuan VO-DINH. *Handbook of Spectroscopy*. 1st edition. Weinheim: WILEY-VCH Verlag GmbH & Co., 2003. ISBN 3-527-29782-0.

[21] STUART, Barbara H. *Infrared Spectroscopy: Fundamentals and Applications*. John Wiley & Sons, 2004. ISBN 9780470011140.

[22] KANIA, Patrik. INFRAČERVENÁ SPEKTROMETRIE. *VŠCHT: Ústav analytické chemie* [online]. Praha, 2007, [cit. 2020-07-21]. Available from: www.vscht.cz/anl/lach1/7_IC.pdf

[23] TOLSTOY, Valeri P., Irina V. CHERNYSHOVA and Valeri A. SKRYSHEVSKY. *Handbook of infrared spectroscopy of ultrathin films*. Hoboken: Wiley-Interscience, 2003. ISBN 047135404X.

[24] HARVEY, David. *Modern analytical chemistry*. Boston: McGraw-Hill, 2000. ISBN 978-0072375473.

[25] SOMMER, Lumír. *Základy analytické chemie*. Brno: VUTIUM, 2000. ISBN 80-214-1742-0.

[26] CECH, V., J. STUDYNKA, B. CECHALOVA, J. MISTRIK and J. ZEMEK. Correlation between mechanical, optical and chemical properties of thin films deposited by PECVD. *Surface and Coatings Technology*. 30 August 2008n. l., **202**(Issues 22–23), 5572-5575. DOI: 10.1016/j.surfcoat.2008.06.031.

[27] NOVOTNÁ, Miroslava. *Laboratoř molekulové spektroskopie: Infračervená spektroskopie* [online]. Praha. VŠCHT, 2010 [cit. 2020-07-21]. Available from: http://lms.vscht.cz/Zverze/Infrared.htm

[28] LIN-VIEN, Daimay. *The Handbook of infrared and Raman characteristic frequencies of organic molecules*. Boston: Academic Press, c1991. ISBN 01-245-1160-0.

[29] BRUKER OPTICS INC. *VERTEX Series Advanced Research FT-IR Spectrometers*. 2010.

[30] DESHMUKH, Shashank S. and Erav E. AVDIL. Investigation of SiO2 plasma enhanced chemical vapor deposition through tetraethoxysilane using attenuated total reflection Fourier transform infrared spectroscopy. *Journal of Vacuum Science and Technology A: Vacuum, Surfaces and Films.* 1995, **13**(5.), 2355-2367. DOI: https://doi.org/10.1116/1.579521.

[31] CASSERLY, THOMAS b. and Karen K. GLEASON. Chemical Vapor Deposition of Organosilicon Thin Films from Methylmethoxysilanes. *Plasme Processe and Polymers*. 2005, **2**(9), 679-687. DOI: https://doi.org/10.1002/ppap.200500055.

[32] STUDYNKA, Jan a Vladimir CECH. Aging of silicon-based dielectric coatings deposited by plasma polymerization. *Thin Solid Films*. **519**(7), 2168-2171. DOI: https://doi.org/10.1016/j.tsf.2010.11.025.

[33] ZAK, Lubos, Erik PLASECH, Vrastislav PERINA a Vladimir CECH. Physicochemical properties of plasma-polymerized tetravinylsilane films controlled by the effective power. *21st International Symposium on Plasma Chemistry (ISPC 21)*. Queensland, Australia: Cairns Convention Centre, 2013.

[34] BUREŠ, Michal. *Studium plazmových produktů pomocí hmotnostní spektrometrie: Study of plasma species by mass spectroscopy*. Brno: Brno University of Technology, Faculty of Chemisty, 2008. Thesis supervisor Prof. RNDr. Vladimír Čech, Ph.D.

[35] KING, S.W., M. FRENCH, J. BIELEFELD and W.A. LANFORD. Fourier transform infrared spectroscopy investigation of chemical bonding in low-k a-SiC:H thin films. *Journal of Non-Crystalline Solids*. 2011, **357**(15), 2970-2983. DOI: https://doi.org/10.1016/j.jnoncrysol.2011.04.001.

[36] HOUDKOVA, Jana, Martin BRANECKY, Tomas PLICHTA, Petr JIRICEK, Jozef ZEMEK and Vladimir CECH. *Chemical depth profile of layered a-CSiO:H nanocomposites*. 2018, **456**. DOI: https://doi.org/10.1016/j.apsusc.2018.06.227.

[37] BRANECKY, Martin, Naghmeh ABOUALIGALEDARI and Vladimir CECH. Plasma Nanotechnology for Controlling Chemical and Physical Properties of Organosilicon Nanocoatings. *Materials Today Communications*. 2020, **24**, 101234. DOI: https://doi.org/10.1016/j.mtcomm.2020.101234.

[38] CECH, Vladimir, Jan STUDYNKA, N. CONTE and V. PERINA. Physicochemical properties of plasma-polymerized tetravinylsilane. *Surface and Coatings Technology*. 2007, **201**(9), 5512-5517. DOI: DOI: 10.1016/j.surfcoat.2006.07.086.

[39] RYU, Soo Ryeon, Isao NODA and Young Mee JUNG. Positional Fluctuation of IR Absorption Peaks: Frequency Shift of a Single Band or Relative Intensity Changes of Overlapped Bands? *American laboratory*. 2011, **43**(4), 40-43.

[40] CECH, Vladimir, Josef ZEMEK and Vrastislav PERINA. Chemistry of Plasma-Polymerized Vinyltriethoxysilane Controlled by Deposition Conditions. *Plasma Processes and Polymer*. 2008, **5**(8), 745-752. DOI: https://doi.org/10.1002/ppap.200800007.

[41] GRILL, Alfred and Deborah A. NEUMAYER. Structure of low dielectric constant to extreme low dielectric constant SiCOH films: Fourier transform infrared spectroscopy characterization. *Journal of Applied Physics* [online]. 2003, **94**(10), 6697 [cit. 2020-07-22]. DOI: https://doi.org/10.1063/1.1618358.

7 ABBREVIATIONS

CVD	Chemical vapor deposition
DC	Direct current
FIR	Far infrared
FTIR	Fourier Transform Infrared Spectroscopy
IR	Infrared spectrum
IRBAS	Software for processing the infrared spectra
MIR	Middle infrared
NIR	Near infrared
OFHC	Oxygen Free High Conductivity
PECVD	Plasma-Enhanced Chemical Vapor Deposition
PLD	Pulsed Laser Deposition
PVD	Physical Vapor Deposition
RF	Radio frequency
TVS	Tetravinylsilane